JOURNAL OF PETROLOGY | VOLUME 48 | NUMBER 2 | PAGES 365–393 | 2007 | doi:10.1093/petrology/egl063

The Role of Pressure in Producing Compositional Diversity in Intraplate Basaltic Magmas

M. L. WHITAKER*, H. NEKVASIL, D. H. LINDSLEY AND N. J. DIFRANCESCO

DEPARTMENT OF GEOSCIENCES, STONY BROOK UNIVERSITY, STONY BROOK, NY 11794-2100, USA

RECEIVED JANUARY 24, 2006; ACCEPTED SEPTEMBER 29, 2006; ADVANCE ACCESS PUBLICATION NOVEMBER 18, 2006

Basaltic magmas found in intraplate suites appear to follow more than one differentiation trend. Many ocean island suites follow the ocean island tholeiitic trend, with the basalts differentiating from olivine tholeiite through basaltic andesite, andesite, and dacite to sodic rhyolite. Many continental intraplate magmatic regimes, such as those of the Snake River Plain and the plutonic sequences associated with massif anorthosites, follow the potassic silica-saturated alkalic trend, in which basalt differentiates from olivine tholeiite through ferrobasalt (jotunite or ferrodiorite), Fe-rich intermediate rocks (trachybasalt or monzonite), and trachyte (syenite) to potassic rhyolites and granites. Crystallization experiments on an olivine tholeiite from the Snake River Plain show that the basaltic portions of the ocean island tholeiitic trend and the potassic silica-saturated alkalic trend (which leads to strong alkali, P, Ti, and Fe enrichment and silica depletion) can arise from the same 'dry' tholeiitic parental magma. These compositional differences are induced by changes in phase equilibria as a function of pressure, with the ocean island tholeiitic series arising from crystal–liquid differentiation at low pressure and the potassic silica-saturated alkalic series arising via differentiation at elevated pressures.

KEY WORDS: *tholeiite differentiation; experimental petrology; phase equilibria; ferrodiorite; ferrobasalt*

INTRODUCTION

Magmatic suites associated with hotspot or continental rift activity commonly contain a wide variety of rocks that are spatially and temporally related (i.e. Carmichael, 1964; Abbott, 1969; Frey *et al.*, 1991; Frost *et al.*, 1993). Nekvasil *et al.* (2000, 2003) have shown that this compositional diversity comprises several distinct trends. Figure 1a shows the three primary compositional trends of bulk-rocks of silica-saturated [in the sense of Yoder & Tilley (1962)] intraplate magmatic suites (Trends 1–3). Trend 1, defined by lavas of the ocean island tholeiitic series, is exemplified by rocks from Easter Island (Baker *et al.*, 1974; Haase *et al.*, 1997), the Galapagos archipelago (Pinzon Island, Baitis & Lindstrom, 1980; Volcan Alcedo, Geist *et al.*, 1995), and the Thingmuli volcano in Iceland (Carmichael, 1964). Bulk compositions of rocks of this series are subalkalic throughout their entire range of compositions (Fig. 1b), and follow the sequence olivine tholeiite–basaltic andesite–andesite (icelandite)–dacite–sodic rhyolite.

Rocks of the potassic silica-saturated alkalic series (Trend 2, Fig. 1a) are found exclusively in continental regimes. This series is exemplified by rocks of hotspot-related large igneous provinces (i.e. Yellowstone–Snake River Plain volcanic province) and the rocks associated with massif anorthosite complexes (excluding the obvious cumulate rocks). This trend is characterized by the tholeiitic nature of the least-evolved mafic rocks, the mildly alkalic nature of its intermediate units, and the potassic nature (i.e. high K_2O/Na_2O ratio) of the silicic rocks. Volcanic suites from this trend make up the sequence tholeiitic basalt–ferrobasalt–trachybasalt–trachyandesite–tristanite–trachyte–potassic rhyolite (Fig. 1b, Leeman *et al.*, 1976; Stout & Nicholls, 1977; Leeman, 1982a; Kuntz *et al.*, 1992; Stout *et al.*, 1994; Frost & Frost, 1997; McCurry *et al.*, 1999, 2006), as seen in the Snake River Plain (SRP). Plutonic equivalents, such as from the Laramie Anorthosite Complex (LAC), follow the series olivine gabbro–ferrodiorite (jotunite)–monzodiorite–monzonite–monzosyenite–syenite–potassic granite (Frost *et al.*, 1993; Scoates *et al.*, 1996; see Frost *et al.*, 1999, fig. 1b).

The potassic silica-saturated alkalic trend can be subdivided into two main segments (Fig. 1c): a silica-depletion

*Corresponding author. Fax: (631) 632-8240.
E-mail: matthew.whitaker@sunysb.edu

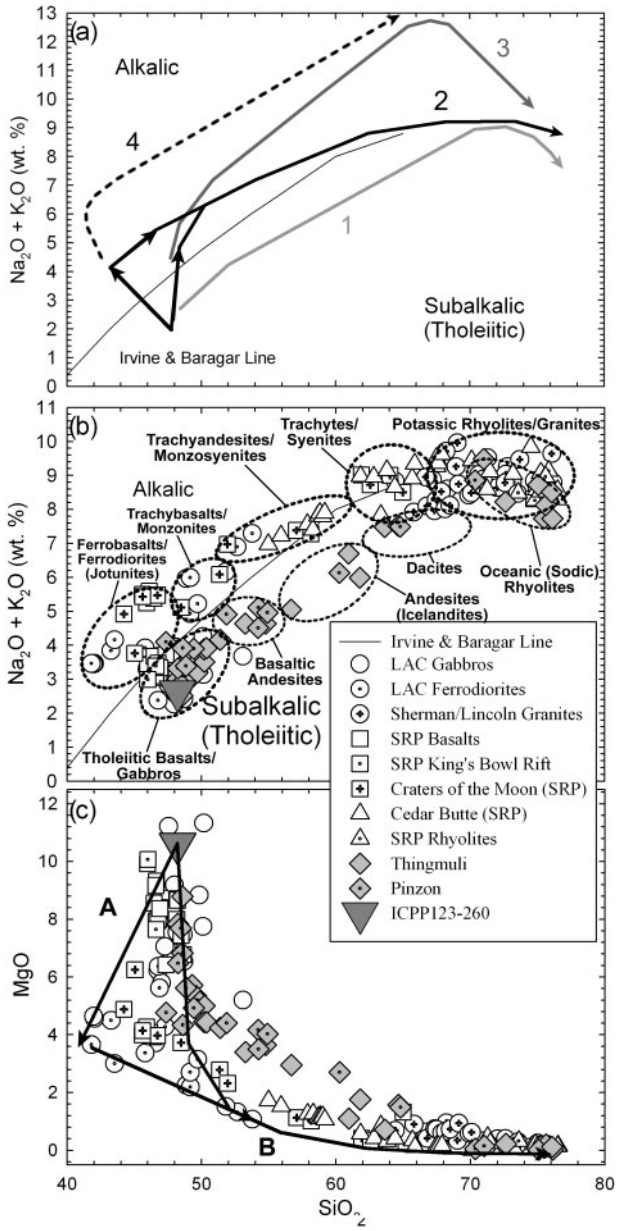

Fig. 1. (a) Total alkalis vs silica variation diagram depicting the three major silica-saturated compositional trends of bulk-rocks in intraplate magmatic suites: (1) ocean island tholeiitic series; (2) potassic silica-saturated alkalic series; (3) silica-saturated sodic alkalic series; (4) the primary silica-undersaturated alkalic series. (b) Total alkalis vs silica variation and (c) MgO vs silica variation in bulk compositions of natural rocks of the potassic silica-saturated alkalic trend (open symbols) from the Snake River Plain (SRP basalts and basalts of the SRP King's Bowl Rift, Kuntz *et al.*, 1992; basalts and intermediate rocks of Craters of the Moon lava field, Leeman *et al.*, 1976; Stout & Nicholls, 1977; Stout *et al.*, 1994; intermediate rocks and rhyolites of Cedar Butte, McCurry *et al.*, 2006; SRP rhyolites, Leeman, 1982b) and non-cumulate rocks of the Laramie Anorthosite Complex (gabbros, Mitchell *et al.*, 1995; ferrodiorites, Mitchell *et al.*, 1996; Sherman–Lincoln granites, Frost *et al.*, 1999), and the rocks of the ocean island tholeiitic trend (gray symbols) from Thingmuli, Iceland (Carmichael, 1964) and Pinzon, Galapagos (Baitis & Lindstrom, 1980). The line separating the alkalic and subalkalic fields is from Irvine & Baragar (1971). All data presented here and in subsequent variation diagrams are normalized to 100% on a volatile-free basis. Compositional fields displaying the rock types of these two series are shown in (b). The silica-depletion segment of the potassic silica-saturated alkalic series is indicated by the arrow marked A in (c); the silica enrichment segment of the series is shown by the arrows marked B in (c). ICPP123-260 (dark gray triangle) is the olivine tholeiite used as the starting material in this study. (Whereas MgO or *mg*-number is typically used to show basalt differentiation, SiO_2 was chosen to emphasize silica variation during differentiation.)

(but not commonly silica-undersaturated) and a silica-enrichment segment. The silica-depletion segment (segment A, Fig. 1c) of this trend begins in the tholeiitic field with the least-evolved mafic rocks and extends toward low-silica, high-Fe–Ti–P ferrobasaltic rocks with decreasing MgO, crossing the subalkalic–alkalic boundary. The silica-enrichment segment begins primarily with the low-silica ferrobasalts and extends through the trachybasalt and trachyandesite fields to trachyte and potassic rhyolite (segment B, Fig. 1c). [Whitaker *et al.* (2006) noted an additional silica-enrichment trend emanating from tholeiite and extending to the more evolved ferrobasalts and on to rhyolite (Fig. 1c).] The high-silica portion of this trend that leads to potassic rhyolite has recently been experimentally investigated (Whitaker *et al.*, 2004, 2006). The work presented here focuses specifically on the compositional diversity of the basaltic rocks.

Trend 3, the sodic silica-saturated alkalic trend, reflects the evolution of lavas from mildly alkalic basalt to alkali-rich sodic rhyolite and is exemplified by lavas from Ascension Island (e.g. Harris, 1983) and the Nandewar Volcano, Australia (e.g. Stolz, 1985). Nekvasil *et al.* (2004) experimentally produced liquids along this trend through crystallization of a mildly alkalic basalt from the Nandewar Volcano at 9·3 kbar with dissolved water content >0·5 wt %. Because of the importance of water to this trend, it will not be discussed further in this paper. Trend 4 is the silica-undersaturated alkalic series, exemplified by rocks from Hawaii (e.g. Frey *et al.*, 1991) and Gough Island (e.g. Leroex, 1985). The rocks of this series have preliminarily been shown to form at higher pressures than those investigated in this study (Filiberto & Nekvasil, 2003), and are the subject of a forthcoming study (Filiberto *et al.*, in preparation).

The liquid line of descent of the basaltic rocks of both the ocean island tholeiitic series and the potassic silica-saturated alkalic series appears to be controlled by crystal–liquid differentiation. Thompson (1975) carried out melting experiments on a tholeiite (6·7 wt % MgO) from the SRP and determined that at pressures between 8 and 12 kbar the liquids produced were similar in composition to the SRP ferrobasalts; Litvin (2002) determined experimentally that the ferrobasalts of the SRP can be reproduced by crystallization of a slightly more primitive

tholeiitic magma (8·6 wt % MgO) at lower crustal pressures (9·3 kbar) under nominally anhydrous (~0·13 wt % H_2O) conditions. Similarly, Scoates *et al.* (1999) showed experimentally that crystallization of tholeiitic high-aluminum olivine gabbro from the LAC under these same conditions can give rise to the ferrodiorites (jotunites) of the anorthosite complexes.

The major and trace element characteristics of rocks of ocean island tholeiitic suites can be accounted for by crystallization of observed phenocryst phases (Baitis & Lindstrom, 1980; Geist *et al.*, 1995). Experimental crystallization of a Kilauea basalt at low pressure (1 kbar) by Spulber & Rutherford (1983) produced a liquid line of descent with similar characteristics to the trend in major element compositions found at Thingmuli. Even in cases where there has been some contamination by crustal material (i.e. Macdonald *et al.*, 1987), the evolutionary trends in major and trace element composition have been shown to be consistent with crystal–liquid differentiation.

A potential link

Many petrologists maintain that the processes or sources that have produced the ocean island tholeiitic series and the potassic silica-saturated alkalic series (Trends 1 and 2, Fig. 1a) must be fundamentally different (i.e. Geist *et al.*, 1995; Frost & Frost, 1997) because the rocks from these suite types are clearly different. The least-evolved members of both suite types, however, are very similar in major element composition (Fig. 1). This similarity, when combined with the experimental and chemical evidence that the rocks within each suite type are related by differentiation, raises the question of whether the same type of parent magma crystallizing under different conditions can produce the major element characteristics of the basaltic rocks of both suite types.

This paper presents new experimental data evaluating the extent of compositional diversity in basaltic liquids that can be produced by crystallization of olivine tholeiite magma at various pressures under 'anhydrous' conditions. Although the primary variable under consideration in this paper is pressure some consideration must be given to oxygen fugacity. In natural rocks of the two suite types there is a difference in oxygen fugacity, with the ocean island tholeiite showing more oxidized compositions. The experiments mimic this difference; the higher pressure experiments were conducted at lower oxygen fugacity than the lower pressure experiments.

Experimental strategy

Experiments were designed to determine the liquid lines of descent of an 'anhydrous' intraplate olivine tholeiite as it ponds and undergoes equilibrium crystallization at various levels within the crust, producing liquids that eventually separate from the crystallized phases before further crystallization, eruption, or final emplacement. The pressures for these experiments were chosen to simulate ponding and crystallization in magma chambers at the base of the average continental crust (9·3 kbar, equivalent to ~30 km), at mid-crustal levels (4·3 kbar, ~15 km), and at sub-volcanic levels ('0 kbar'). Also, intermediate pressures between these were chosen (6·8 and 2·8 kbar), corresponding to the top and bottom of a mid-crustal high-density layer at ~10–20 km depth along the axis of the Snake River Plain (Sparlin *et al.*, 1982; Peng & Humphreys, 1998).

EXPERIMENTAL METHODS

Starting material

The starting material for the experiments was a natural olivine tholeiite from the eastern Snake River Plain (ICPP123 260, abbreviated hereafter as I260; see Table 1), selected because of its high *mg*-number, high MgO content, low Ni content (87 ppm), lack of abundant phenocrysts, and minor amounts of alteration. The low bulk-rock Ni content and the compositional similarity of the groundmass and phenocrystic olivine suggest that the high Mg content of sample I260 is not the result of accumulated olivine, and that it could represent a liquid.

Sample I260 does not fall on the same Ni vs Mg trend as the vast majority of other SRP basalts; however, most basaltic rocks from the SRP have abundant olivine phenocrysts. Because the olivine–melt partition coefficients for these two elements are vastly different (Duke, 1976;

Table 1: Composition of starting material [ICPP123-260 (I260), olivine tholeiite]

Component	Content (wt%)
SiO_2	47·53
TiO_2	1·43
Al_2O_3	15·03
FeO_T	10·53
MnO	0·16
MgO	10·46
CaO	10·57
Na_2O	2·18
K_2O	0·42
P_2O_5	0·26
Total	98·58
mg-no.[1]	0·68
H_2O in glass (wt%)[2]	0·35[3] (0·05)[4]

[1] *mg*-number = molar Mg/(Mg + Fe^{2+}) assuming an Fe^{2+}/Fe_T ratio of 0·85.
[2] Measured by FTIR on fused sample.
[3] Structurally bound water in natural sample.
[4] After drying at 800°C.

Takahashi, 1978), accumulation of olivine would alter their relative proportions in the bulk-rock, and thus may explain why sample I260, which contains very little phenocrystic olivine, falls off of this compositional trend, but still probably represents a liquid.

Sample I260 is significantly less evolved (10·62 wt % MgO) than the samples used in previous experimental studies and typical of the tholeiite (non-primitive) commonly found in these types of suites. Sample I260 is a mildly vesicular rock containing ~2 vol. % phenocrystic olivine, and lesser amounts of plagioclase phenocrysts. The groundmass consists primarily of plagioclase, clinopyroxene and olivine, with minor amounts of Fe–Ti oxides, quenched glass, iddingsite, and trace amounts of apatite. Additional information on this rock has been given by Reed *et al.* (1997; sample ICPP123-79).

The rock sample was crushed and ground to yield a fine homogeneous powder with an average grain size of a few microns. This powder, when fused at 1320°C and 9·3 kbar in a graphite capsule, contains 0·35 wt % H_2O as determined by micro-Fourier Transform Infrared Spectroscopy (FTIR). For the 'anhydrous' experiments reported in this paper, as much of this water as possible was removed, as described below.

Piston-cylinder experiments

For each experiment, the powdered rock was dried after loading into a graphite capsule by placing the capsule into a silica glass tube with an Fe° oxygen 'getter' and glass spacer to keep them separated. This assembly was evacuated and heated for 20 min in a vertical furnace. The drying geometry ensured that the capsule was heated to 800°C while the Fe° 'getter' was at 600°C, thereby preventing oxidation of the sample material during drying. After cooling, the sample was removed and placed into the cell assembly, loaded into the 1/2 inch piston-cylinder apparatus, and pressurized to prevent re-adsorption of water. The bulk water content of the dried sample was found by FTIR analysis of a fused sample to be 0·05 wt %.

The cell assembly for the piston-cylinder experiments consisted of a low-porosity (~14 %) $BaCO_3$ outer sleeve, into which a graphite furnace was inserted along with dried mullite spacers and crushable MgO discs. The graphite capsule in this assembly was in direct contact with the graphite sleeve, thereby effectively becoming part of the furnace assembly. An insulating alumina disc separated the thermocouple from the graphite capsule. The temperature of the experiment was both controlled and monitored by a $Pt–Pt_{90}Rh_{10}$ thermocouple. This assembly has a temperature gradient of +12°C from the thermocouple to the center of the capsule at 9·3 kbar, and a gradient of +14°C at 4·3 kbar. The temperatures reported here are those at the hotspot of the sample. Pressures reported include a −0·7 kbar correction based on the subsolidus reaction Mg-cordierite = Sapphirine + Quartz (Newton *et al.*, 1974) at 7 kbar.

Because the experimental charges were housed in graphite, their fO_2 was partially controlled by the graphite–CO–CO_2 (GCO) buffer. However, because there was no vapor phase evident in our experiments, the GCO buffer provides only an upper limit to fO_2 (Eugster & Skippen, 1967). The actual fO_2 is affected by the bulk composition of the sample (especially the Fe^{3+}/Fe^{2+} ratio) within the graphite capsule. Whenever an appropriate assemblage was present, the fO_2 was calculated using QUILF assemblage of olivine, pyroxene, and ilmenite and the technique of Andersen *et al.* (1993). For the piston-cylinder experiments, the fO_2 of the system was computed (using the QUILF) to be ~2·5 log units below fayalite–magnetite–quartz (FMQ) buffer at all pressures. However, an appropriate assemblage was available only at low temperatures for this starting material. To assess the fO_2 at higher temperatures, calibration experiments were conducted at 1200°C by adding sufficient spinel ($Usp_{95}Mt_5$) and ilmenite ($Hem_{20}Ilm_{80}$) to I260 powder to ensure that two oxides remained after melting and crystallization. The resulting oxide pairs yielded fO_2 values 1·5 log units (9·3 kbar) and 2·3 log units (4·3 kbar) below the FMQ buffer. These calibration experiments provide, however, only an upper limit to the fO_2, because the bulk oxide compositions were reduced during reaction, indicating that they effectively added oxygen to the sample, raising its initial Fe^{3+}/Fe^{2+} ratio.

Crystallization experiments were conducted using the piston-out method in which the pressure was slowly raised to a value approximately 2 kbar greater than the desired pressure while still at room temperature, then the sample was heated to the melting temperature (1300–1320°C) before decreasing the overpressure. The sample remained at this melting temperature and pressure for 2 h to ensure complete fusion, then was rapidly cooled to the final crystallization temperature of the experiment, where the sample remained for 2–3 days. Each experiment was quenched by turning off the power, resulting in an initial cooling rate of ~100°C/s.

Experiments at '0 kbar'

Low-pressure experiments were conducted in a Pt-wound vertical quench furnace using $Au_{80}Pd_{20}$ capsules inserted into silica glass tubes. To compensate for potential Fe loss to the capsule, 6 relative wt % Fe° sponge (the amount of Fe lost to the capsule in a test run) was added to the rock powder. The Fe°-enriched I260 powder was loaded into each capsule and the top was crimped shut. The sample was then dried by placing it into a silica glass tube with a glass spacer, drawing out a capillary just above the spacer, placing a piece of Fe° oxygen 'getter' into the tube above the capillary, and drying under the conditions described for the piston-cylinder experiments. After drying, and

with the sample still under vacuum, the silica-glass capillary was sealed, severed, and worked into a loop, producing an evacuated ampoule that could be hung in the vertical quench furnace.

The Pt-wound quench furnaces used for these experiments were restricted to temperatures of 1250°C or below. As the liquidus temperature of the I260 starting material is higher than this maximum, the evacuated ampoule containing the sample material was first placed in a Deltech furnace at 1280°C for 2–3 h to ensure complete melting, and then air-quenched. The ampoule was then suspended in the quench furnace by a fine Pt wire, heated to 1250°C, and then allowed to cool to its final crystallization temperature at a rate of 1°C/min, where it remained for 2–3 days. To quench the charge, the fine Pt wire holding it in the furnace was fused, causing the sample to drop into a cold water bath. The integrity of the ampoule after the experiment was tested by comparing pre- and post-experiment weights, and by heating the end of the ampoule near the spacer to check the quality of the vacuum. Only experiments that passed both the weighing and vacuum tests are reported here.

At the temperature of each experiment, the pressure in the tube must equal the sum of the vapor pressures of the phases. This sum is not known, but must be less than the tensile strength of the silica-glass tubes (~3 bar). These experiments are referred to here as '0 kbar' experiments because of this uncertainty. The fO_2 of these experiments was assessed using the technique of Andersen *et al.* (1993) whenever the QUILF mineral assemblage olivine + pyroxene + spinel ± ilmenite was present. Such calculations yielded values of ~1–2 log units above FMQ. The fO_2 of these experiments is not greatly different from that found in the rocks of Thingmuli (Carmichael, 1964), which Frost & Lindsley (1992) calculated to be 1 log unit below to 1 log unit above FMQ.

Analytical techniques

The major element compositions of all phases present in experimental run products were determined by electron microprobe. Analytical conditions were 15 kV and 10 nA, with an 11 μm × 11 μm rastered beam whenever grain size permitted. Counting was for 30 s or to 40 000 counts for all elements except Si (40 s or 111 111 counts) and Al (40 s or 62 500 counts), and the PAP correction routine was used. Standards were microcline for K and Si, anorthite for Ca and Al, ilmenite for Fe and Ti, albite for Na, forsterite for Mg, apatite for P, and rhodonite for Mn. Care was taken to avoid alkali loss (especially from glass) by analyzing Na and K first and exposing the analyzed area to the beam for as short a time period as possible prior to analysis. Alkali loss from glass compositions was signaled by the appearance of normative corundum (Co); the absence of Co in all glass compositions reported here suggests that alkali loss has been minimal. All pyroxene, olivine and oxide analyses were projected through QUILF (Andersen *et al.*, 1993) and checked for equilibrium between these phases, and the fO_2 of the system was calculated when the assemblages permitted.

The IgPet Program Suite (Carr, 2002) was used to calculate molar norms of all residual liquids and pyroxenes as well as to conduct mass-balance calculations using a least-squares routine. These least-squares calculations yielded phase proportions (in wt %) and helped ensure that no phases were overlooked during microprobe analysis. Only those combinations of phases in a single experiment that yielded sums of the squares of the residuals less than 0·15 are reported here.

The water contents of glasses were measured by analyzing doubly polished wafers of the experimental run products with micro-IR spectroscopy using the Nicolet 20SXB FTIR spectrometer and Spectra Tech IR Plan microscope at the American Museum of Natural History. The density of the glasses and the total water concentrations were calculated using the methods of Dixon *et al.* (1995) and Mandeville *et al.* (2002).

EXPERIMENTAL RESULTS

The run products of experiments contained variable amounts of crystalline phases and glass. There was little to no compositional zoning present in the crystals with the exception of augite, which commonly displayed significant variation in non-quadrilateral components, especially Ti and Al. Only experiments that produced homogenous residual glass are reported here.

Phase relations

The assemblages crystallizing from dry olivine tholeiite are strongly pressure-dependent (Tables 2–6, Fig. 2). Figure 3 shows the computed abundances of phases present in the experiments. At all pressures, olivine is the liquidus phase; at '0 kbar' it is joined by a spinel phase that persists over the entire range of temperatures explored. At 9·3 kbar, sub-calcic augite is the next phase to appear, followed by plagioclase and eventually ilmenite in the lowest-temperature experiment. At pressures below 9·3 kbar, plagioclase joins the crystallizing assemblage before augite (not sub-calcic); ilmenite is absent at 6·8 and 2·8 kbar even in the lowest-temperature experiments. Plagioclase becomes the dominant phase in the assemblage at lower temperatures at all pressures except 9·3 kbar where it is in equal abundance with augite.

Figure 4 shows olivine and pyroxene compositions as projected into the pyroxene quadrilateral through QUILF (Andersen *et al.*, 1993) using the method of Lindsley & Anderson (1983, pp. A894–A895). The compositions of the olivines are only slightly influenced by the pressure at which they crystallized, with the liquidus olivine being slightly more magnesian at low pressure. In constrast,

Table 2: Representative mineral compositions of I260 experimental assemblages with 0·05 bulk wt% H_2O at 9·3 kbar

Phase:	Olivine	Olivine	Augite	Olivine	Augite	Olivine	Augite	Plag	Olivine	Augite
Experiment (no.):	I260-65	I260-62	I260-62	I260-58	I260-58	I260-50	I260-50	I260-50	I260-55	I260-55
Temperature (°C):	1280	1260	1260	1240	1240	1220	1220	1220	1200	1200
SiO_2	38·71	38·77	48·90	38·19	49·83	37·34	48·54	52·67	36·61	47·18
TiO_2	0·04	0·02	0·71	0·00	0·75	0·02	1·03	0·09	0·06	1·32
Al_2O_3	0·08	0·08	8·62	0·08	8·11	0·08	7·93	29·38	0·11	9·03
FeO	15·29	17·05	6·96	18·91	7·29	24·07	9·45	0·25	27·02	10·48
MnO	0·19	0·18	0·16	0·19	0·22	0·24	0·25	0·00	0·31	0·24
MgO	42·28	41·43	17·72	40·61	16·81	36·45	15·79	0·14	33·63	14·12
CaO	0·32	0·30	13·86	0·30	14·87	0·31	14·30	12·49	0·35	14·94
Na_2O	0·01	0·01	0·44	0·01	0·45	0·01	0·55	4·15	0·00	0·64
K_2O	0·00	0·00	0·01	0·01	0·01	0·00	0·01	0·26	0·00	0·00
P_2O_5	0·08	0·10	0·05	0·08	0·05	0·04	0·03	0·02	0·09	0·03
Total	96·99	97·94	97·43	98·37	98·38	98·56	97·88	99·45	98·18	97·98
Comp. (mol%)	$Fo_{83}(La_{0·4})$	$Fo_{81}(La_{0·4})$	$En_{66}Wo_{20}$	$Fo_{79}(La_{0·4})$	$En_{62}Wo_{22}$	$Fo_{73}(La_{0·4})$	$En_{58}Wo_{22}$	$An_{62}(Or_2)$	$Fo_{69}(La_{0·5})$	$En_{55}Wo_{24}$

Phase:	Plag	Spinel	Olivine	Augite	Plag	Spinel	Olivine	Augite	Plag	Ilmenite
Experiment (no.):	I260-55	I260-55	I260-54	I260-54	I260-54	I260-54	I260-61	I260-61	I260-61	I260-61
Temperature (°C):	1200	1200	1180	1180	1180	1180	1160	1160	1160	1160
SiO_2	53·57	0·18	36·14	46·78	53·91	0·42	35·92	47·15	54·36	0·14
TiO_2	0·11	0·77	0·06	1·98	0·10	0·81	0·08	2·24	0·08	52·32
Al_2O_3	28·61	59·94	0·09	9·20	28·16	60·10	0·10	8·64	28·35	0·88
FeO	0·44	19·21	28·97	10·29	0·53	19·19	30·32	11·18	0·31	36·46
MnO	0·03	0·10	0·34	0·23	0·06	0·16	0·34	0·17	0·01	0·36
MgO	0·12	14·99	31·79	13·32	0·11	14·98	30·71	13·43	0·08	6·60
CaO	11·51	0·10	0·33	15·23	11·13	0·20	0·35	14·73	10·86	0·44
Na_2O	4·55	0·00	0·03	0·66	4·46	0·03	0·01	0·67	4·60	0·02
K_2O	0·45	0·00	0·00	0·02	0·61	0·01	0·00	0·01	0·79	0·02
P_2O_5	0·04	0·00	0·27	0·03	0·02	0·02	0·29	0·03	0·05	0·02
Total	99·42	95·30	98·02	97·74	99·08	95·91	98·12	98·24	99·48	97·25
Comp. (mol%)	$An_{57}(Or_3)$	n.a.	$Fo_{66}(La_{0·5})$	$En_{53}Wo_{25}$	$An_{56}(Or_4)$	n.a.	$Fo_{64}(La_{0·5})$	$En_{51}Wo_{25}$	$An_{54}(Or_5)$	$Ilm_{98}Hem_2$

n.a., not applicable.

the compositions of the pyroxenes are strongly dependent upon pressure, particularly the wollastonite component, as pyroxenes formed at higher pressures have higher Al_2O_3 and Na_2O, and lower CaO than those formed at lower pressures. At 9·3 kbar, the augite compositions lie in the range Wo_{20}–Wo_{25} (increasing with decreasing temperature; Fig. 4a), wherease at lower pressures the Wo content of the pyroxenes is significantly higher (Fig. 4b–e). The augites that crystallized at 9·3 kbar (Fig. 4a) lie in the augite + pigeonite region of the pyroxene quadrilateral (Lindsley, 1983, fig. 9c, p. 485). This is a computational artifact arising from the high alumina content of the pyroxene (8–9 wt % Al_2O_3). The projection scheme of Lindsley & Anderson (1983) 'over-corrects' for the presence of Al in the pyroxene, thereby driving the calculated Wo content of the 9·3 kbar pyroxenes into that two-phase region.

The relationships between coexisting feldspars and liquids are shown in Fig. 5. For this figure, the molar normative feldspar components (An, Ab, Or) were normalized to unity for the residual liquids, feldspars, and pyroxenes. (The pyroxenes were included in this projection to meet mass-balance constraints.) The compositions of the feldspars formed during these experiments are highly

Table 3: Representative mineral compositions of I260 experimental assemblages with 0·05 bulk wt% H_2O at 6·8 kbar

Phase:	Olivine	Olivine	Olivine	Plag	Olivine	Plag	Augite	Olivine
Experiment (no.):	I260-194	I260-193	I260-204	I260-204	I260-188	I260-188	I260-188	I260-191
Temperature (°C):	1260	1240	1220	1220	1200	1200	1200	1180
SiO_2	38·87	38·60	38·82	50·37	37·81	51·61	50·01	37·49
TiO_2	0·03	0·06	0·07	0·06	0·05	0·08	1·06	0·05
Al_2O_3	0·12	0·10	0·13	30·60	0·09	30·14	4·99	0·10
FeO	14·60	16·56	17·90	0·23	21·35	0·43	7·40	24·34
MnO	0·20	0·22	0·26	0·00	0·30	0·01	0·19	0·28
MgO	44·27	42·65	42·01	0·20	38·22	0·23	15·65	35·98
CaO	0·34	0·35	0·38	14·15	0·41	13·67	18·60	0·48
Na_2O	0·01	0·01	0·03	3·29	0·00	3·56	0·41	0·02
K_2O	0·00	0·01	0·00	0·16	0·00	0·19	0·00	0·01
P_2O_5	0·11	0·20	0·15	0·00	0·06	0·05	0·03	0·05
Total	98·55	98·76	99·74	99·06	98·30	99·97	98·34	98·79
Comp. (mol%)	$Fo_{84}(La_{0·5})$	$Fo_{82}(La_{0·5})$	$Fo_{80}(La_{0·5})$	$An_{70}(Or_1)$	$Fo_{76}(La_{0·6})$	$An_{67}(Or_1)$	$En_{53}Wo_{34}$	$Fo_{72}(La_{0·7})$

Phase:	Plag	Augite	Olivine	Plag	Augite	Olivine	Plag	Augite
Experiment (no.):	I260-191	I260-191	I260-186	I260-186	I260-186	I260-206	I260-206	I260-206
Temperature (°C):	1180	1180	1160	1160	1160	1140	1140	1140
SiO_2	52·05	48·69	37·52	51·98	49·06	36·74	52·89	48·00
TiO_2	0·13	1·82	0·08	0·12	1·61	0·13	0·13	2·56
Al_2O_3	29·71	6·37	0·07	29·30	5·04	0·12	28·38	6·58
FeO	0·70	7·39	25·62	0·61	8·86	29·35	1·19	9·28
MnO	0·01	0·18	0·39	0·01	0·23	0·39	0·03	0·30
MgO	0·41	14·04	34·20	0·21	14·23	32·28	0·83	12·80
CaO	12·86	19·10	0·47	12·84	18·43	0·45	12·00	18·37
Na_2O	3·83	0·41	0·01	4·03	0·40	0·03	4·04	0·56
K_2O	0·23	0·02	0·01	0·30	0·01	0·00	0·45	0·05
P_2O_5	0·03	0·07	0·03	0·03	0·02	0·09	0·02	0·14
Total	99·94	98·08	98·41	99·43	97·87	99·58	99·95	98·63
Comp. (mol%)	$An_{64}(Or_1)$	$En_{50}Wo_{35}$	$Fo_{70}(La_{0·7})$	$An_{63}(Or_2)$	$En_{48}Wo_{35}$	$Fo_{66}(La_{0·7})$	$An_{60}(Or_3)$	$En_{46}Wo_{35}$

dependent upon the pressure of crystallization, which is in good agreement with the results of Fram & Longhi (1992). The anorthite content of the first-formed plagioclase increases with decreasing pressure, from An_{62} at 9·3 kbar to An_{78} at '0 kbar'. The higher-pressure feldspars are also more Or-rich ($Or_{2–5}$ at 9·3 kbar) than the lower-pressure feldspars ($Or_{<1–1}$ at '0 kbar').

Liquid evolution

The compositions of residual liquids produced by crystallization of I260 are highly dependent upon pressure (Tables 7–11 and Figs 6–12). Residual liquids produced at 9·3 kbar become strongly depleted in silica and enriched in total alkalis, crossing the boundary into the alkalic field (Table 7, Fig. 6). The strong silica depletion of the residual liquids is accompanied by depletion in MgO and CaO, and strong enrichment in FeO_T, TiO_2, and P_2O_5, thereby producing ferrobasaltic (jotunitic) compositional characteristics (Fig. 7). Both Al_2O_3 and Na_2O initially increase strongly, but eventually exhibit marked decreases as plagioclase joins the crystallizing assemblage. K_2O steadily increases nearly incompatibly throughout the crystallization sequence.

The residual liquids produced at 6·8 kbar show similar, but less pronounced, silica depletion and alkali enrichment; the residual liquids still move from the tholeiitic to the alkalic

Table 4: Representative mineral compositions of I260 experimental assemblages with 0·05 bulk wt% H_2O at 4·3 kbar

Phase:	Olivine	Olivine	Olivine	Olivine	Plag	Olivine	Plag	Augite	Olivine
Experiment (no.):	I260-78	I260-81	I260-82	I260-84	I260-84	I260-83	I260-83	I260-83	I260-77
Temperature (°C):	1260	1240	1220	1200	1200	1180	1180	1180	1160
SiO_2	39·29	38·93	38·41	38·24	49·98	38·15	51·58	50·13	36·57
TiO_2	0·01	0·03	0·03	0·04	0·09	0·06	0·13	1·28	0·10
Al_2O_3	0·26	0·09	0·06	0·13	31·60	0·08	30·48	5·15	0·08
FeO	14·07	15·85	16·07	18·07	0·20	22·67	0·81	6·97	25·52
MnO	0·17	0·22	0·22	0·21	0·00	0·33	0·00	0·11	0·34
MgO	41·92	42·84	42·04	40·90	0·22	37·15	0·25	14·92	34·22
CaO	0·41	0·30	0·34	0·37	14·40	0·59	13·70	19·44	0·50
Na_2O	0·11	0·00	0·02	0·01	3·11	0·02	3·43	0·30	0·00
K_2O	0·03	0·00	0·00	0·00	0·14	0·00	0·19	0·00	0·00
P_2O_5	0·29	0·11	0·13	0·12	0·04	0·02	0·04	0·04	0·04
Total	96·56	98·36	97·31	98·09	99·79	99·06	100·60	98·33	97·37
Comp. (mol%)	$Fo_{84}(La_{0·6})$	$Fo_{83}(La_{0·4})$	$Fo_{82}(La_{0·5})$	$Fo_{80}(La_{0·5})$	$An_{72}(Or_1)$	$Fo_{74}(La_{0·8})$	$An_{68}(Or_1)$	$En_{51}Wo_{36}$	$Fo_{70}(La_{0·7})$

Phase:	Plag	Augite	Olivine	Plag	Augite	Olivine	Plag	Augite	Ilmenite
Experiment (no.):	I260-77	I260-77	I260-79	I260-79	I260-79	I260-201	I260-201	I260-201	I260-201
Temperature (°C):	1160	1160	1140	1140	1140	1120	1120	1120	1120
SiO_2	51·96	48·50	36·53	52·25	49·57	36·12	52·78	47·07	0·67
TiO_2	0·15	1·68	0·09	0·18	1·82	0·12	0·14	2·77	52·45
Al_2O_3	29·49	4·79	0·13	28·96	4·48	0·18	28·29	5·38	1·09
FeO	0·74	8·13	28·09	0·80	9·08	29·35	0·74	10·60	35·86
MnO	0·00	0·14	0·35	0·00	0·21	0·34	0·02	0·25	0·42
MgO	0·41	14·08	32·17	0·56	14·61	32·27	0·18	12·71	6·91
CaO	12·91	18·66	0·50	12·67	18·40	0·44	11·65	18·85	0·58
Na_2O	3·77	0·36	0·03	3·95	0·43	0·03	4·53	0·41	0·09
K_2O	0·26	0·01	0·00	0·35	0·03	0·01	0·54	0·02	0·02
P_2O_5	0·05	0·05	0·02	0·05	0·06	0·06	0·03	0·05	0·00
Total	99·73	96·39	97·91	99·77	98·68	98·93	98·91	98·11	98·09
Comp. (mol%)	$An_{64}(Or_2)$	$En_{48}Wo_{36}$	$Fo_{67}(La_{0·7})$	$An_{63}(Or_2)$	$En_{48}Wo_{35}$	$Fo_{66}(La_{0·9})$	$An_{57}(Or_3)$	$En_{43}Wo_{38}$	$Ilm_{98}Hem_2$

field (Table 8, Fig. 6). Figure 8 shows that there is sufficient depletion in MgO accompanied by enrichment in FeO_T, TiO_2, and P_2O_5, to again lead to the production of ferro-basaltic liquids. Liquids produced by crystallization of I260 at 4·3 kbar show only mild silica depletion during crystallization and less enrichment in FeO_T, TiO_2, and P_2O_5 than at higher crystallization pressure; the liquids still cross into the alkalic field (Table 9, Figs 6 and 9). The decrease in Na_2O in the lowest temperature residual liquids, although still apparent, is much less pronounced than that observed at both 9·3 and 6·8 kbar. When crystallizing at 2·8 kbar, this olivine tholeiite magma evolves from tholeiitic to mildly alkalic at nearly constant silica content (Table 10, Fig. 6). The FeO_T, TiO_2, and P_2O_5 enrichment is less pronounced than at higher pressures, and the decrease in Na_2O that was observed in the residual liquids of the lowest temperature experiments at higher pressures is not exhibited (Fig. 10).

Residual liquids produced at '0 kbar' trend directly toward silica enrichment (Table 11, Fig. 6). Although alkalis are also enriched along this liquid line of descent, the liquid never crosses the subalkalic–alkalic boundary of Irvine & Baragar (1971). The melts remain tholeiitic (sub-alkalic) as the magma evolves to basaltic andesite

Table 5: Representative mineral compositions of I260 experimental assemblages with 0·05 bulk wt% H_2O at 2·8 kbar

Phase:	Olivine	Olivine	Olivine	Plag	Olivine	Plag	Olivine	Plag	Augite
Experiment (no.):	I260-205	I260-196	I260-179	I260-179	I260-195	I260-195	I260-200	I260-200	I260-200
Temperature (°C):	1240	1220	1200	1200	1180	1180	1160	1160	1160
SiO_2	39·60	39·12	39·32	48·73	38·53	50·14	37·96	51·45	49·23
TiO_2	0·04	0·04	0·05	0·06	0·04	0·08	0·07	0·11	1·73
Al_2O_3	0·06	0·11	0·07	31·46	0·07	30·58	0·06	30·05	5·07
FeO	14·71	15·66	16·69	0·35	18·47	0·35	23·62	0·51	7·08
MnO	0·23	0·17	0·20	0·00	0·23	0·01	0·38	0·00	0·18
MgO	45·13	43·98	42·21	0·22	41·26	0·25	37·02	0·23	14·68
CaO	0·32	0·36	0·34	15·41	0·42	14·70	0·42	13·83	20·14
Na_2O	0·01	0·00	0·02	2·60	0·02	3·05	0·00	3·53	0·35
K_2O	0·01	0·00	0·01	0·09	0·00	0·11	0·00	0·17	0·01
P_2O_5	0·06	0·13	0·00	0·01	0·02	0·04	0·01	0·02	0·04
Total	100·16	99·55	98·92	98·94	99·05	99·30	99·54	99·89	98·49
Comp. (mol%)	$Fo_{84}(La_{0·4})$	$Fo_{83}(La_{0·5})$	$Fo_{81}(La_{0·5})$	$An_{76}(Or_{<1})$	$Fo_{79}(La_{0·6})$	$An_{72}(Or_{<1})$	$Fo_{73}(La_{0·6})$	$An_{68}(Or_1)$	$En_{49}Wo_{38}$

Phase:	Olivine	Plag	Augite	Olivine	Plag	Augite
Experiment (no.):	I260-198	I260-198	I260-198	I260-207	I260-207	I260-207
Temperature (°C):	1140	1140	1140	1120	1120	1120
SiO_2	37·39	52·17	49·43	37·27	53·35	48·83
TiO_2	0·03	0·13	2·15	0·12	0·23	2·67
Al_2O_3	0·05	29·58	4·49	0·10	28·83	5·13
FeO	26·09	0·66	7·97	28·92	0·83	8·69
MnO	0·41	0·03	0·15	0·40	0·01	0·21
MgO	35·35	0·23	13·95	33·51	0·32	12·94
CaO	0·43	13·23	20·36	0·48	12·67	20·62
Na_2O	0·03	3·78	0·32	0·04	4·11	0·37
K_2O	0·01	0·26	0·01	0·01	0·32	0·02
P_2O_5	0·05	0·05	0·04	0·10	0·06	0·07
Total	99·84	100·12	98·86	100·95	100·73	99·55
Comp. (mol%)	$Fo_{70}(La_{0·6})$	$An_{65}(Or_1)$	$En_{46}Wo_{40}$	$Fo_{67}(La_{0·7})$	$An_{62}(Or_2)$	$En_{43}Wo_{40}$

composition with early increases in CaO, TiO_2, FeO_T, and Al_2O_3; these elements become depleted as crystallization continues, with Al_2O_3 leveling off again at the highest degrees of crystallinity.

In experiments where plagioclase was crystallizing, the crystallization pressure had a strong effect on the liquid line of descent (Fig. 5). At low pressure, the high abundance of plagioclase, together with its higher An content, results in greater An depletion and Ab enrichment with increasing differentiation. The incremental change in liquid compositions produced by the change in mineral assemblage at the five experimental pressures can be seen in Figs 6 and 12.

DISCUSSION

Implications for the potassic silica-saturated alkalic series

Snake River Plain

By simulating the process whereby an olivine tholeiite magma would pond and undergo equilibrium crystallization at various levels within the crust, liquid compositions were produced that span much of the diversity in major element bulk-rock composition of basaltic rocks found in the natural suites from the SRP. The experimental mineral assemblages that give rise to these residual liquids can also

Table 6: Representative mineral compositions[1] of I260 experimental assemblages at '0 kbar' in $Au_{80}Pd_{20}$

Phase:	Olivine	Cr-Spinel	Olivine	Cr-Spin	Olivine	Cr-Spinel[2]	Plag	Olivine	Cr-Spinel	Plag	Olivine	Cr-Spinel[2]	Plag	Augite
Experiment (no.):	I260-38	I260-38	I260-15	I260-15	I260-30	I260-30	I260-30	I260-16	I260-16	I260-16	I260-20	I260-20	I260-20	I260-20
Temperature (°C):	1250	1250	1230	1230	1200	1200	1200	1180	1180	1180	1150	1150	1150	1150
SiO_2	39·38	0·20	39·80	0·40	39·51	1·91	48·68	39·52	0·89	49·46	38·65	11·19	50·60	49·05
TiO_2	0·04	0·94	0·07	0·94	0·05	1·15	0·04	0·03	1·88	0·07	0·03	4·48	0·12	1·33
Al_2O_3	0·09	25·50	0·11	25·35	0·12	27·78	31·36	0·06	21·44	31·21	0·05	11·90	30·00	4·40
FeO	12·26	22·85	12·36	22·86	13·94	26·61	0·82	15·14	33·36	0·63	18·99	41·26	0·82	6·76
MnO	0·17	0·12	0·16	0·17	0·23	0·16	0·00	0·26	0·21	0·00	0·29	0·30	0·01	0·22
MgO	47·05	14·20	46·07	14·23	45·07	13·28	0·22	44·21	12·25	0·23	39·65	7·90	0·29	14·65
CaO	0·34	0·36	0·40	0·34	0·39	0·75	15·64	0·37	0·54	14·93	0·42	2·51	14·23	20·36
Na_2O	0·01	0·02	0·04	0·04	0·00	0·10	2·36	0·02	0·15	2·71	0·03	0·63	3·16	0·27
K_2O	0·01	0·01	0·00	0·02	0·00	0·03	0·09	0·00	0·01	0·10	0·00	0·18	0·14	0·01
P_2O_5	0·05	0·02	0·01	0·01	0·03	0·02	0·03	0·02	0·03	0·00	0·09	0·09	0·06	0·06
Total	99·38	64·21	99·01	64·35	99·33	71·78	99·23	99·63	70·75	99·34	98·19	80·43	99·43	97·10
Comp. (mol%)	$Fo_{87}(La_{0·5})$	n.a.	$Fo_{86}(La_{0·5})$	n.a.	$Fo_{85}(La_{0·5})$	n.a.	$An_{78}(Or_{<1})$	$Fo_{83}(La_{0·5})$	n.a.	$An_{75}(Or_{<1})$	$Fo_{78}(La_{0·6})$	n.a.	$An_{71}(Or_1)$	$En_{49}Wo_{39}$

Phase:	Olivine	Plag	Augite	Ti-Mag[2]	Olivine	Plag	Augite	Ti-Mag	Olivine	Plag	Augite	Ti-Mag	Ilmenite
Experiment (no.):	I260-24	I260-24	I260-24	I260-24	I260-27	I260-27	I260-27	I260-27	I260-31[3]	I260-31[3]	I260-31[3]	I260-31[3]	I260-31[3]
Temperature (°C):	1130	1130	1130	1130	1100	1100	1100	1100	1080	1080	1080	1080	1080
SiO_2	38·17	50·26	48·96	5·22	37·41	50·58	47·55	0·44	37·47	51·28	47·69	0·16	0·08
TiO_2	0·09	0·22	1·46	6·90	0·05	0·08	2·16	16·00	0·09	0·10	2·15	15·78	42·21
Al_2O_3	0·19	28·55	3·96	7·92	0·71	29·43	4·75	3·45	0·04	29·22	4·27	3·09	0·61
FeO	20·27	1·53	8·46	59·90	24·86	1·17	9·54	65·93	25·21	1·11	10·85	67·83	46·22
MnO	0·24	0·00	0·15	0·23	0·35	0·03	0·27	0·33	0·42	0·03	0·30	0·33	0·29
MgO	39·08	0·46	14·47	5·36	35·39	0·24	12·95	4·91	35·02	0·24	13·02	4·90	5·49
CaO	0·46	13·79	19·30	1·76	0·51	13·71	19·92	0·30	0·38	13·33	19·02	0·32	0·25
Na_2O	0·04	3·14	0·27	0·28	0·09	3·38	0·34	0·02	0·01	3·53	0·39	0·01	0·02
K_2O	0·02	0·22	0·02	0·04	0·01	0·23	0·02	0·04	0·00	0·20	0·05	0·03	0·01
P_2O_5	0·09	0·06	0·08	0·02	0·11	0·03	0·08	0·05	0·04	0·03	0·09	0·02	0·01
Total	98·64	98·22	97·13	87·63	99·48	98·87	97·56	91·46	98·68	99·07	97·82	92·47	95·17
Comp. (mol%)	$Fo_{77}(La_{0·6})$	$An_{70}(Or_1)$	$En_{47}Wo_{38}$	$Usp_{26}Mt_{74}$	$Fo_{71}(La_{0·7})$	$An_{68}(Or_1)$	$En_{44}Wo_{40}$	$Usp_{50}Mt_{50}$	$Fo_{71}(La_{0·6})$	$An_{67}(Or_1)$	$En_{44}Wo_{38}$	$Usp_{48}Mt_{52}$	$Ilm_{76}Hem_{24}$

[1]Significant Cr peaks observed in EDS spectra of Cr-spinels and Ti-magnetites, which probably accounts for low totals.
[2]Oxide phase is too small to be analyzed without significant overlap; analysis included for completeness.
[3]The phases from the 1080°C experiment at '0 kbar' may not reflect an equilibrium assemblage.
n.a., not applicable.

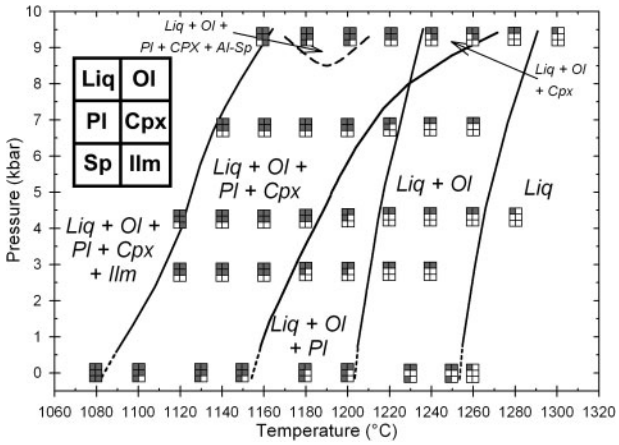

Fig. 2. *P–T* diagram showing phase assemblages for all experiments conducted in this study. Shaded areas within the rectangles indicate phases present; legend is given at the left side. Liq, liquid; Ol, olivine; Pl, plagioclase; Cpx, clinopyroxene; Sp, spinel; Ilm, ilmenite.

be used for comparison with the natural assemblages. However, such comparison must be made with caution. The bulk lava compositions are considered here to represent residual liquid removed from the assemblage crystallizing at higher pressure. Upon ascent, this liquid will probably crystallize to some extent; therefore, the existing mineral assemblages in the rock are likely to represent primarily the phases crystallizing from these residual liquids at the final ponding or crystallization pressure prior to eruption rather than those crystallizing at higher pressure. Comparison of the natural and experimental mineral assemblages, however, should provide insight into this final pressure of crystallization of the SRP magmas.

Olivine tholeiites and related basalts from the SRP are commonly reported to contain up to 20 vol. % olivine phenocrysts with less abundant phenocrystic plagioclase and rare clinopyroxene. The cores of olivine phenocrysts in these basalts range from Fo_{85} to Fo_{60}, and plagioclase phenocrysts range in composition from An_{80} to An_{60} (Leeman, 1982*b*). The more evolved basaltic and ferrobasaltic rocks from the Craters of the Moon (COM) lava field in the SRP commonly contain phenocrysts of olivine and plagioclase with minor amounts of pyroxene locally. The compositions of the olivine phenocrysts range from Fo_{72} in the basalts to Fo_5 in the 'ferrolatites' (trachybasalts–trachyandesites), and the plagioclase phenocrysts range from An_{63} to An_{30} over the range in bulk-rock composition (Leeman *et al.*, 1976).

The least-evolved phenocrysts in these rocks are nearly identical in composition to the same phases found in the highest temperature experiment at 9·3 kbar that contains both olivine and plagioclase (Fo_{73} and An_{62}), but there is a greater difference between the assemblages in the more evolved compositions. The major difference between the experimental mineral assemblages that led to the strong Fe–Ti–P enrichment seen in the bulk compositions of the natural rocks and the natural phenocryst assemblages described in SRP–COM basaltic rocks is the presence of abundant clinopyroxene in the former. The lack of abundant pyroxene phenocrysts in the SRP–COM rocks has led previous workers (e.g. Leeman, 1982*b*) to postulate that these rocks must have formed by differentiation in a magma chamber shallow enough to allow olivine and plagioclase to crystallize without clinopyroxene in the assemblage. Mass-balance calculations to assess the relationship between the bulk compositions of SRP rocks by crystallization have been plagued by this lack of clinopyroxene phenocrysts in the natural samples. Leeman *et al.* (1976) found it impossible to generate the bulk compositions of the ferrobasalts of the COM suite from the average McKinney basalt composition (Leeman & Vitaliano, 1976) by crystallizing the low-pressure (1 bar) phenocryst assemblage of olivine, plagioclase and spinel. However, crystallization of the mineral assemblage experimentally observed by Thompson (1975) in his 8 kbar experiments on an SRP basalt (olivine, clinopyroxene, and plagioclase) could give liquids that were similar in composition to COM ferrobasalts. Similarly, Stout *et al.* (1994) also found that they needed a significant amount of clinopyroxene (nearly twice the amount of olivine crystallized) in their calculations to obtain a good match for deriving a COM ferrobasalt from an SRP basalt.

The requirement for significant amounts of clinopyroxene in these mass-balance calculations is consistent with the experimental implications that a higher-pressure history is needed to produce ferrobasaltic liquids from the tholeiite. The absence of high-pressure phenocrystic clinopyroxene crystals in the lavas can be explained simply—they were left behind along with other higher-pressure crystalline phases during ascent of the residual liquid. The greatest similarity in mineral assemblage (relative abundances and compositions) between those produced experimentally and those observed in rocks from the Snake River Plain–Craters of the Moon is is seen in the lower-pressure experimental assemblages. This suggests that following ascent of these residual liquids generated at depth, lower-pressure crystallization took place prior to eruption at the surface. Because the bulk compositions retain their higher-pressure signature, the final magma ascent did not involve the separation of liquid from the low-pressure crystalline assemblage.

It is worth noting here that the results obtained in our 9·3 kbar experiments are very different from those obtained by Villiger *et al.* (2004), who conducted equilibrium and fractional 'crystallization' experiments on a tholeiitic basalt at 1·0 GPa (10 kbar). Whereas we find significant silica depletion in our residual liquids at this

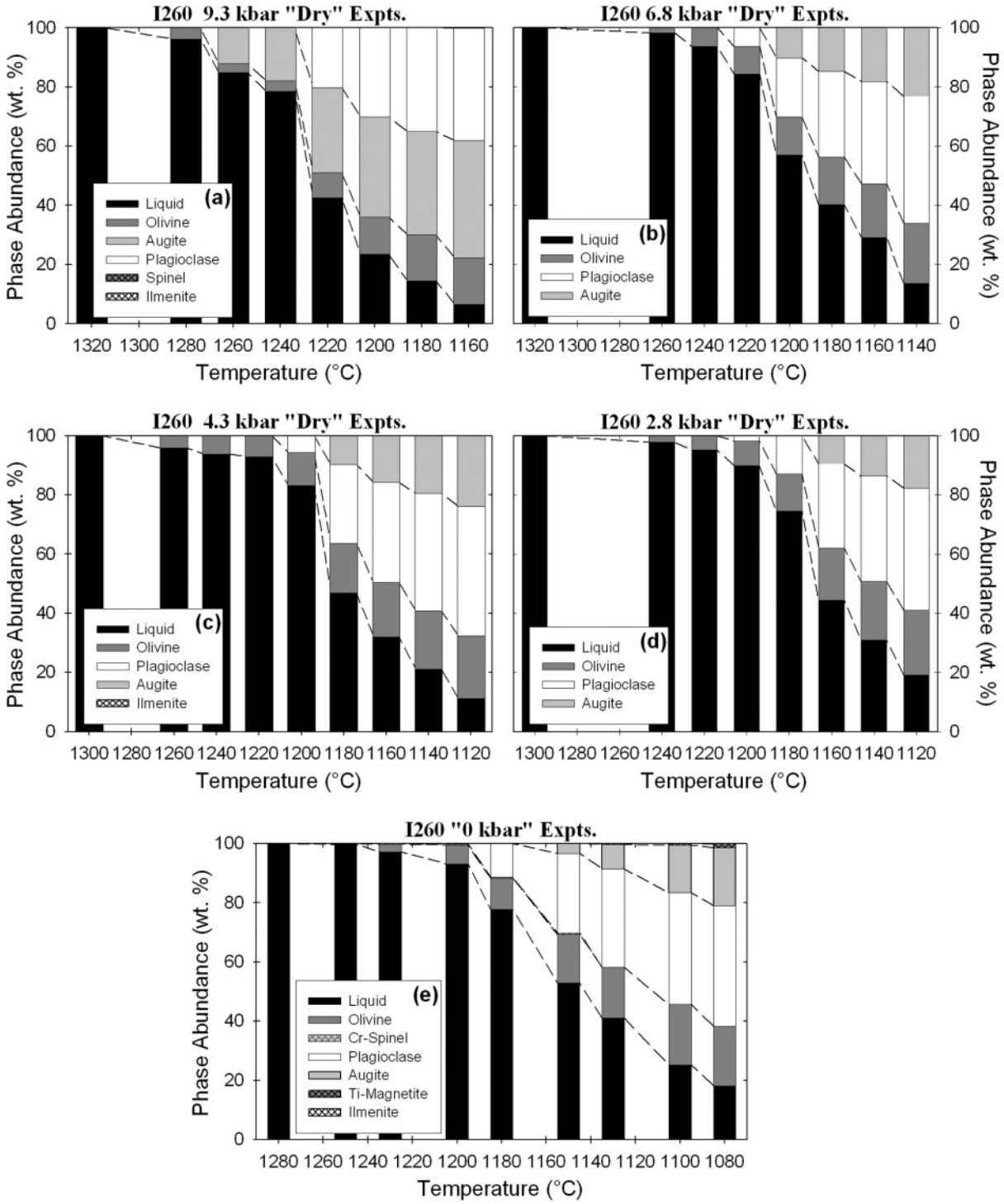

Fig. 3. Variation in phase abundances (wt%) with temperature of experimental run products of 'dry' I260 at (a) 9·3 kbar, (b) 6·8 kbar, (c) 4·3 kbar, (d) 2·8 kbar, and (e) '0 kbar'.

pressure, the residual liquids in their experiments showed silica enrichment. One possible reason for this disparity lies in the differences in experimental approach; our experiments were true crystallization experiments in which the bulk material was melted completely and then allowed to crystallize. The experiments of Villiger *et al.* (2004) were melting experiments in which the charges were taken directly to the desired

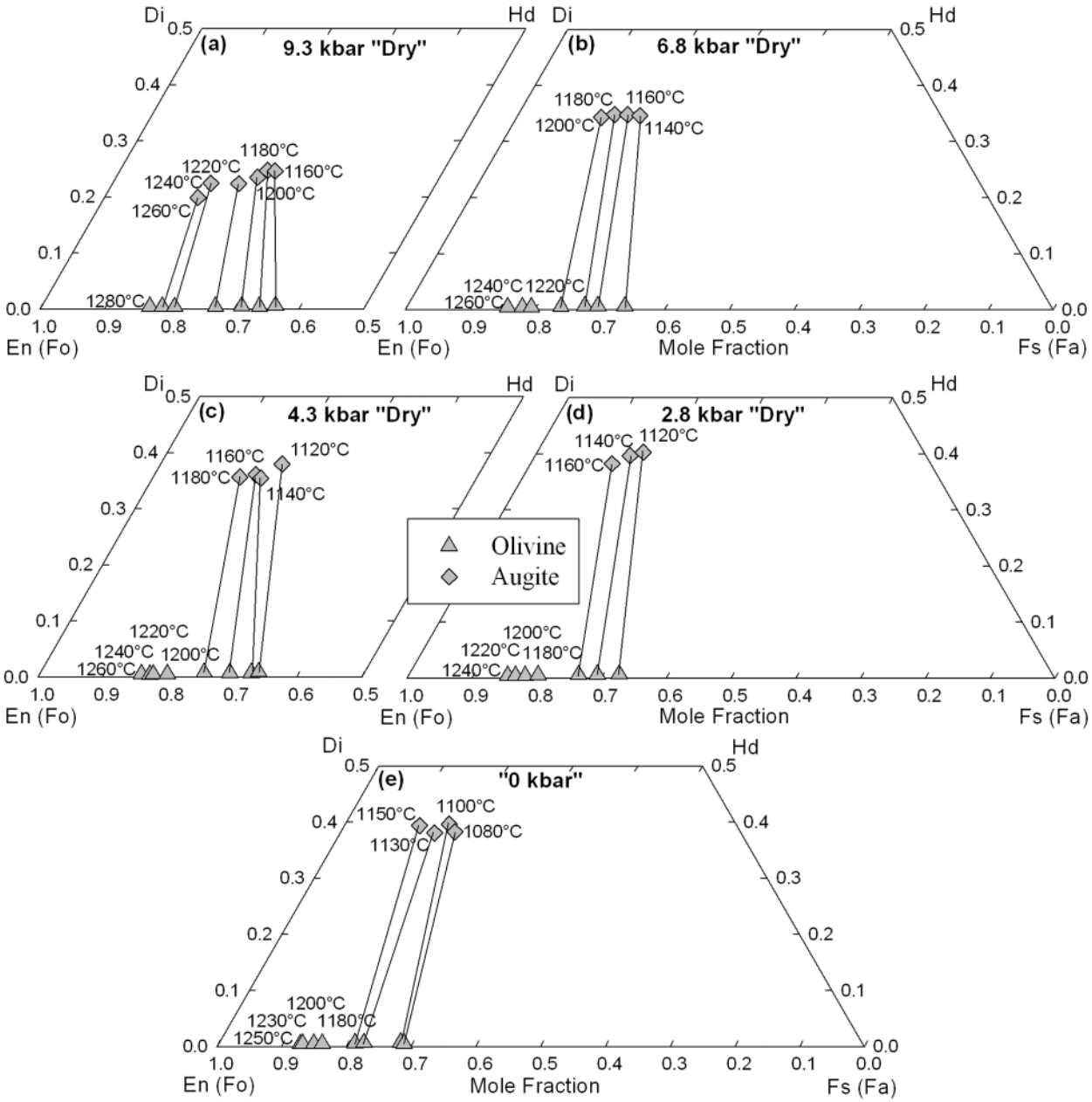

Fig. 4. QUILF projections of olivine (gray triangles) and pyroxene (gray diamonds) compositions from experimental run products of 'dry' I260 at (a) 9·3 kbar, (b) 6·8 kbar, (c) 4·3 kbar, (d) 2·8 kbar, and (e) '0 kbar'. Tie-lines connect coexisting phases. Experimental temperatures are indicated.

crystallization temperature. In the former experiments, both using natural rock powder and melting the starting material above, but close to, the liquidus temperature facilitated nucleation. The latter approach involves melting a metastable assemblage of oxides only at the 'crystallization' temperature (Villiger *et al.*, 2004). This may have led to the nucleation problems that were encountered (involving plagioclase and even olivine in some experiments).

Plagioclase crystallization plays an important role in driving residual liquids toward silica depletion. Inhibition of plagioclase nucleation at this pressure (10 kbar) would contribute to the silica enrichment exhibited by the residual liquids of Villiger *et al.* (2004), or at the very least strongly decrease the amount of silica depletion that might occur. Another possible reason for the discrepancy in residual melt compositions lies in the possible presence

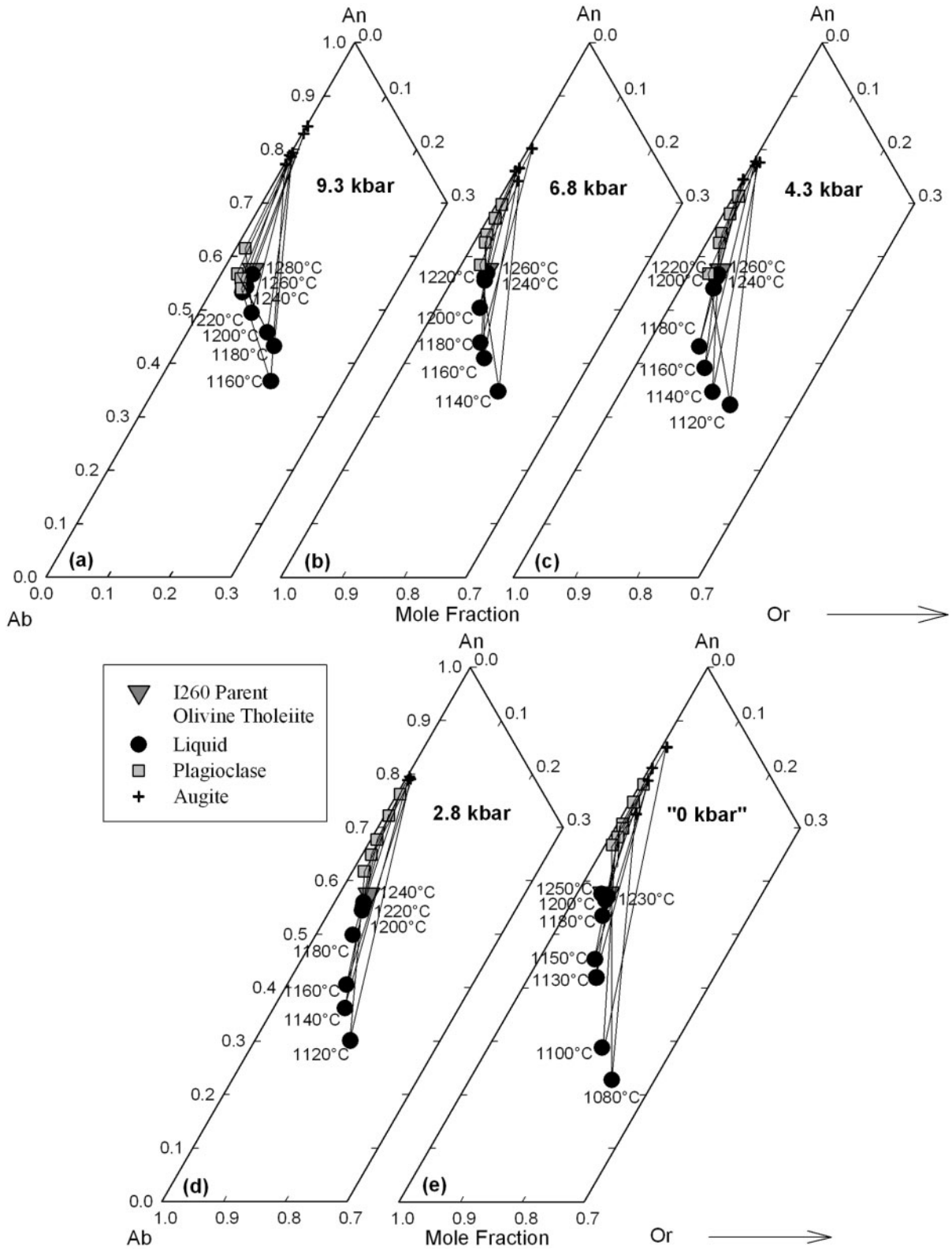

Fig. 5. Plagioclase compositions (gray squares) and molar normative feldspar constituents of glass (black circles) and pyroxene (black crosses) of I260 'dry' experiments at (a) 9·3 kbar, (b) 6·8 kbar, (c) 4·3 kbar, (d) 2·8 kbar, and (e) '0 kbar'. Tie-lines connect coexisting phases. Temperatures of experiments are indicated.

Table 7: Representative residual liquid compositions of I260 experiments with 0·05 bulk wt% H_2O[1] at 9·3 kbar

Experiment (no.):	I260-65	I260-62	I260-58	I260-50
Mode (wt%):	Gl 96·2%, Ol 3·8%	Gl 84·8%, Ol 3·0%, Aug 12·2%	Gl 78·5%, Ol 3·5%, Aug 18·0%	Gl 42·6%, Ol 8·4%, Aug 28·8%, Pl 20·2%
Temperature (°C):	1280	1260	1240	1220
SiO_2	47·12	46·04	47·05	45·08
TiO_2	1·50	1·63	1·76	2·47
Al_2O_3	15·66	16·10	16·81	15·90
FeO	10·37	10·49	11·10	13·21
MnO	0·13	0·11	0·22	0·18
MgO	9·12	8·12	7·59	6·46
CaO	10·93	10·21	10·18	9·13
Na_2O	2·32	2·57	2·77	3·04
K_2O	0·48	0·51	0·53	0·81
P_2O_5	0·26	0·34	0·30	0·50
Total	97·88	96·13	98·30	96·77
mg-no.	0·65	0·62	0·59	0·51
H_2O in glass (wt%)[1]	0·05	0·06	0·06	0·11
Crystallinity (wt%)	3·8	15·2	21·5	57·4
S.S.R.	0·05	0·04	0·11	0·03

Experiment (no.):	I260-55	I260-54	I260-61
Mode (wt%):	Gl 23·4%, Ol 12·6%, Aug 33·8%, Pl 30·2%, Sp (trace)	Gl 14·5%, Ol 15·5%, Aug 34·9%, Pl 35·1%, Sp (trace)	Gl 6·8%, Ol 15·7%, Aug 39·4%, Pl 37·9%, Ilm 0·2%
Temperature (°C):	1200	1180	1160
SiO_2	43·81	41·88	41·01
TiO_2	3·37	4·57	6·11
Al_2O_3	15·35	14·62	13·38
FeO	14·66	15·13	17·04
MnO	0·18	0·25	0·23
MgO	5·77	5·45	4·13
CaO	8·44	8·14	8·75
Na_2O	3·25	3·02	2·69
K_2O	1·15	1·35	1·64
P_2O_5	0·75	1·27	2·66
Total	96·75	95·67	97·64
mg-no.	0·45	0·43	0·34
H_2O in glass (wt%)	0·21[1]	0·34[2]	0·74[2]
Crystallinity (wt%)	76·6	85·5	93·2
S.S.R.	0·07	0·01	0·00

[1]Measured by FTIR.
[2]Calculated based on bulk water content and degree of crystallinity.
*S.S.R., sum of squared residuals.

Table 8: Representative residual liquid compositions of I260 experiments with 0·05 bulk wt% H_2O[1] at 6·8 kbar

Experiment (no.):	I260-194	I260-193	I260-204	I260-188
Mode (wt%):	Gl 98·2%, Ol 1·8%	Gl 93·7%, Ol 6·3%	Gl 84·3%, Ol 9·3%, Pl 6·4%	Gl 56·9%, Ol 12·9%, Pl 20·0%, Aug 10·2%
Temperature (°C):	1260	1240	1220	1200
SiO_2	47·54	48·04	47·77	47·32
TiO_2	1·52	1·62	1·82	2·35
Al_2O_3	15·13	15·78	15·84	15·17
FeO	10·57	10·24	10·57	12·14
MnO	0·15	0·15	0·16	0·19
MgO	9·80	8·20	7·76	6·81
CaO	10·80	11·13	11·24	10·43
Na_2O	2·24	2·39	2·43	2·61
K_2O	0·44	0·46	0·51	0·66
P_2O_5	0·26	0·27	0·29	0·42
Total	98·44	98·27	98·39	98·08
mg-no.	0·66	0·63	0·61	0·54
H_2O in glass (wt%)[1]	0·05	0·05	0·07	0·10
Crystallinity (wt%)	1·8	6·3	15·7	43·1
S.S.R.	0·03	0·05	0·09	0·03

Experiment (no.):	I260-191	I260-186	I260-206
Mode (wt%):	Gl 40·2%, Ol 16·1%, Pl 28·9%, Aug 14·8%	Gl 29·1%, Ol 18·1%, Pl 34·6%, Aug 18·2%	Gl 13·5%, Ol 20·3%, Pl 43·0%, Aug 23·2%
Temperature (°C):	1180	1160	1140
SiO_2	46·68	45·38	44·48
TiO_2	2·76	3·24	5·66
Al_2O_3	14·20	14·03	12·90
FeO	13·14	13·85	14·96
MnO	0·21	0·22	0·26
MgO	6·10	5·35	4·95
CaO	9·99	9·48	9·11
Na_2O	2·74	3·20	2·82
K_2O	0·96	1·07	1·56
P_2O_5	0·51	0·59	1·19
Total	97·28	96·39	97·89
mg-no.	0·49	0·45	0·41
H_2O in glass (wt%)[2]	0·12	0·17	0·37
Crystallinity (wt%)	58·8	70·9	86·5
S.S.R.	0·06	0·12	0·09

[1]Measured by FTIR.
[2]Calculated based on bulk water content and degree of crystallinity.

of water; the experiments Villiger *et al.* conducted were referred to as 'nominally anhydrous,' but water content was not specified. As Whitaker *et al.* (2006) determined, the addition of even small amounts of water to a tholeiitic magma at these pressures can cause the residual liquids to evolve toward silica enrichment rather than depletion. Silica enrichment would also be enhanced by the loss of Fe to the Pt lining of the graphite capsule reported by Villiger *et al.* (2004).

Table 9: Representative residual liquid compositions of I260 experiments with 0·05 bulk wt% H_2O[1] at 4·3 kbar

Experiment (no.):	I260-78	I260-81	I260-82	I260-84
Mode (wt%):	Gl 95·8%, Ol 4·2%	Gl 93·8%, Ol 6·2%	Gl 92·9%, Ol 7·1%	Gl 83·1%, Ol 11·1%, Pl 5·8%
Temperature (°C):	1260	1240	1220	1200
SiO_2	47·05	46·97	47·48	47·70
TiO_2	1·50	1·58	1·57	1·73
Al_2O_3	15·66	16·22	16·31	15·88
FeO	10·32	10·06	10·10	10·17
MnO	0·16	0·11	0·15	0·19
MgO	8·97	8·29	7·92	7·00
CaO	10·96	11·16	11·17	11·48
Na_2O	2·37	2·42	2·45	2·54
K_2O	0·48	0·47	0·46	0·52
P_2O_5	0·28	0·27	0·28	0·27
Total	97·75	97·54	97·88	97·49
mg-no.	0·65	0·63	0·62	0·59
H_2O in glass (wt%)[1]	0·05	0·05	0·06	0·08
Crystallinity (wt%)	4·2	6·2	7·1	16·9
S.S.R.	0·05	0·11	0·06	0·05

Experiment (no.):	I260-83	I260-77	I260-79	I260-201
Mode (wt%):	Gl 46·9%, Ol 16·6%, Pl 26·7%, Aug 9·8%	Gl 32·0%, Ol 18·4%, Pl 33·9%, Aug 15·7%	Gl 21·1%, Ol 19·7%, Pl 39·7%, Aug 19·5%	Gl 11·2%, Ol 21·2%, Pl 43·7%, Aug 23·8%, Ilm 0·1%
Temperature (°C):	1180	1160	1140	1120
SiO_2	47·66	46·18	45·99	46·15
TiO_2	2·75	3·36	4·33	5·21
Al_2O_3	14·07	13·80	13·34	13·59
FeO	12·55	13·02	13·69	13·57
MnO	0·22	0·20	0·20	0·13
MgO	6·00	5·23	4·72	4·37
CaO	10·68	9·91	9·25	8·88
Na_2O	2·89	3·05	3·03	3·05
K_2O	0·78	1·04	1·37	1·80
P_2O_5	0·46	0·67	0·96	1·18
Total	98·05	96·47	96·89	97·94
mg-no.	0·50	0·46	0·42	0·40
H_2O in glass (wt%)	0·11[1]	0·16[2]	0·24[2]	0·42[2]
Crystallinity (wt%)	53·1	68·0	78·9	88·8
S.S.R.	0·04	0·06	0·04	0·13

[1]Measured by FTIR.
[2]Calculated based on bulk water content and degree of crystallinity.

Villiger *et al.* (2004) compared their experimental results with pMELTS calculations (Ghiorso *et al.*, 2002) and found that there was very poor agreement between the two. Our 9·3 kbar experiments, on the other hand, are in good agreement with the results of pMELTS calculations conducted using I260 at 10 kbar, which also show a strong silica depletion, Fe–Ti–P-enrichment trend in the residual liquid. MELTS calculations (Ghiorso & Sack, 1995) are not appropriate at this pressure.

Table 10: Representative residual liquid compositions of I260 experiments with 0·05 bulk wt% H_2O[1] at 2·8 kbar

Experiment (no.):	I260-205	I260-196	I260-179	I260-195
Mode (wt%):	Gl 97·8%, Ol 2·2%	Gl 95·2%, Ol 4·8%	Gl 89·8%, Ol 8·4%, Pl 1·8%	Gl 74·5%, Ol 12·6%, Pl 12·9%
Temperature (°C):	1240	1220	1200	1180
SiO_2	48·08	47·94	48·07	47·81
TiO_2	1·47	1·56	1·63	1·89
Al_2O_3	15·39	15·74	16·16	14·86
FeO	10·50	10·29	10·16	10·91
MnO	0·16	0·19	0·20	0·16
MgO	9·80	8·85	7·72	7·01
CaO	10·98	11·15	11·39	11·58
Na_2O	2·36	2·45	2·57	2·66
K_2O	0·43	0·46	0·50	0·56
P_2O_5	0·27	0·27	0·28	0·28
Total	99·43	98·90	98·67	97·71
mg-no.	0·66	0·64	0·61	0·57
H_2O in glass (wt%)[1]	0·05	0·05	0·06	0·08
Crystallinity (wt%)	2·2	4·8	10·2	25·5
S.S.R.	0·02	0·03	0·04	0·07

Experiment (no.):	I260-200	I260-198	I260-207
Mode (wt%):	Gl 44·4%, Ol 17·7%, Pl 28·4%, Aug 9·5%	Gl 31·0%, Ol 19·7%, Pl 35·6%, Aug 13·7%	Gl 19·2%, Ol 21·9%, Pl 41·3%, Aug 17·6%
Temperature (°C):	1160	1140	1120
SiO_2	47·79	47·35	48·01
TiO_2	2·85	3·42	4·17
Al_2O_3	13·95	13·37	13·25
FeO	12·55	13·41	13·39
MnO	0·17	0·22	0·23
MgO	5·73	5·18	4·81
CaO	10·72	10·15	9·57
Na_2O	3·07	3·12	3·47
K_2O	0·88	1·05	1·42
P_2O_5	0·52	0·74	0·86
Total	98·22	98·01	99·18
mg-no.	0·49	0·45	0·43
H_2O in glass (wt%)[2]	0·11	0·16	0·26
Crystallinity (wt%)	55·6	69·0	80·8
S.S.R.	0·10	0·08	0·08

[1]Measured by FTIR.
[2]Calculated based on bulk water content and degree of crystallinity.

Because our experiments were equilibrium crystallization experiments, the liquids produced should be identical to those produced by equilibrium partial melting under the same conditions of pressure, fO_2, and bulk water content. None of these experiments were able to produce liquids close to rhyolite in composition; therefore, these results do not support generation of the low-silica rhyolites at low melt fractions (<10 %) by partial melting of essentially anhydrous gabbro at any pressure within the crust (Christiansen & McCurry, 2006).

Table 11: Representative residual liquid compositions of I260 experiments at '0 kbar' in $Au_{80}Pd_{20}$

Experiment (no.):	I260-38	I260-15	I260-30	I260-16
Mode (wt%):	Gl 99·7%, Ol 0·1%, Cr-Sp 0·2%	Gl 97·3%, Ol 2·5% Cr-Sp 0·2%	Gl 93·2%, Ol 6·3%, Cr-Sp 0·3%, Pl 0·2%	Gl 77·8%, Ol 10·5%, Cr-Sp 0·4%, Pl 11·3%
Temperature (°C):	1250	1230	1200	1180
SiO_2	47·15	47·12	47·34	48·17
TiO_2	1·50	1·49	1·66	1·85
Al_2O_3	14·74	15·36	15·67	14·52
FeO	10·36	10·23	10·07	11·11
MnO	0·16	0·17	0·14	0·19
MgO	10·21	9·46	8·05	7·40
CaO	10·32	10·82	11·29	11·34
Na_2O	2·18	2·24	2·34	2·32
K_2O	0·35	0·47	0·48	0·55
P_2O_5	0·26	0·24	0·29	0·33
Total	97·22	97·59	97·33	97·75
mg-no.	0·67	0·66	0·63	0·58
Crystallinity (wt%)	0·3	2·7	6·8	22·2
S.S.R.	0·04	0·04	0·06	0·01

Experiment (no.):	I260-20	I260-24	I260-27	I260-31
Mode (wt%):	Gl 52·9%, Ol 16·4%, Cr-Sp 0·5%, Pl 26·9%, Aug 3·3%	Gl 41·0%, Ol 17·2%, Pl 33·2%, Aug 8·3%, Ti-Mt 0·3%	Gl 25·2%, Ol 20·4%, Pl 37·8%, Aug 16·0%, Ti-Mt 0·6%	Gl 18·2%, Ol 20·0%, Pl 40·8%, Aug 19·6%, Ti-Mt 1·3%, Ilm 0·1%
Temperature (°C):	1150	1130	1100	1080
SiO_2	48·10	47·99	50·03	52·01
TiO_2	2·82	3·13	4·45	3·68
Al_2O_3	12·78	12·42	12·06	12·29
FeO	12·44	13·41	11·78	10·29
MnO	0·20	0·20	0·17	0·20
MgO	6·25	5·66	4·47	3·85
CaO	11·20	10·21	7·99	7·06
Na_2O	2·44	2·50	2·99	3·29
K_2O	0·74	0·89	1·61	2·14
P_2O_5	0·47	0·56	1·08	1·34
Total	97·43	96·96	96·63	96·15
mg-no.	0·51	0·47	0·44	0·44
Crystallinity (wt%)	47·1	59·0	74·8	81·8
S.S.R.	0·05	0·02	0·09	0·01

The liquids produced experimentally at 9·3 kbar are in good agreement with the ferrobasalts found in the COM suite (and some ferrodiorites from the Laramie Anorthosite Complex), whereas the liquids produced at pressures from 6·8 to 2·8 kbar are better matches for the basaltic rocks found elsewhere in the SRP. Separation of residual liquids following extensive crystallization within the crust would leave behind a large quantity of mafic minerals. Perhaps the high-density layers found at ~10–20 km depth in the SRP (Sparlin *et al.*, 1982; Peng & Humphreys, 1998) represent accumulated crystals left behind during ascent of residual liquid following crystallization, or acted as barriers to upwelling magmas during ascent and facilitated ponding at elevated pressure.

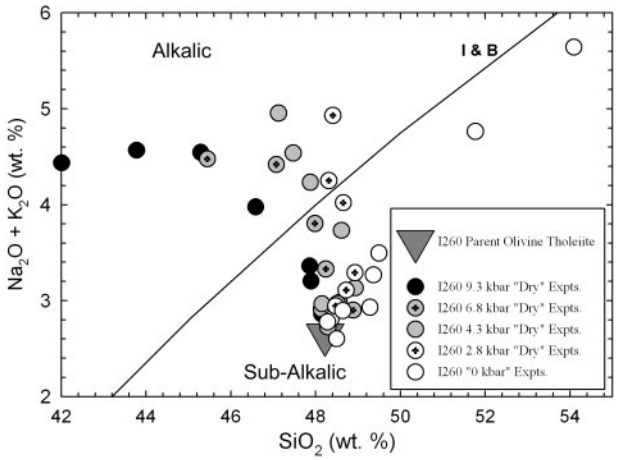

Fig. 6. Total alkalis vs silica variation of experiments at 9·3 kbar (black circles), 6·8 kbar (gray circles with crosshairs), 4·3 kbar (gray circles), 2·8 kbar (open circles with crosshairs), and '0 kbar' (open circles). The line (I & B) separating the alkalic and subalkalic fields is from Irvine & Baragar (1971).

When compared with the natural rocks (Figs 7–10), it appears that the compositional diversity between mafic rocks in large igneous provinces such as the SRP could be caused by tapping of residual liquids formed by crystal–liquid differentiation at a variety of pressures.

Laramie Anorthosite Complex

Whereas much of the compositional diversity observed in the bulk compositions of the gabbroic and dioritic rocks of the LAC has been reproduced in the residual liquids of these experiments over the range of intra-crustal pressures explored, the experimental crystallization path at 9·3 kbar (Figs 6–7) leads to the strong silica depletion and Fe–Ti–P enrichment of residual liquids as they evolve from gabbroic to ferrodioritic (jotunitic) compositions. Liquids strikingly similar to some of the high-aluminum gabbros (HAGs) generally considered to be parental to anorthosite formation (Mitchell *et al.*, 1995) are produced by crystallization of dry olivine tholeiite at 9·3 kbar. The natural gabbros, however, span a large range in alumina content. Those that are higher in alumina than the experimental residual liquids have trace element signatures suggesting excess plagioclase component, perhaps owing to the resorption of accumulated plagioclase during ascent (Mitchell *et al.*, 1995). In general, however, the high alumina contents of our experimental liquids suggest that resorption of accumulated plagioclase is not required to produce many of the observed HAGs.

These experiments support the hypothesis of Mitchell *et al.* (1996) that the ferrodiorites of the LAC represent the liquid complement to the anorthosite and formed by crystallization of a parental magma similar in composition to the LAC Hi-Al gabbros. This support arises from three primary observations. First, experimental liquids residual to tholeiite–HAG crystallization are strikingly similar to the ferrodiorites (Mitchell *et al.*, 1996) with their low silica and alumina, and very high FeO_T, TiO_2, and P_2O_5. Second, plagioclase is a volumetrically abundant phase during high-pressure (9·3 kbar) crystallization of this tholeiite. Finally, the composition of the plagioclase crystallizing at the stage when the residual liquid attains a ferrodioritic composition is very similar to that found in the anorthosite bodies of the LAC. Plagioclase in the anorthosites of the LAC generally ranges from An_{60} to An_{40} (Frost *et al.*, 1993), which is consistent with the experimental values, An_{62}–An_{54}. (The plagioclase produced in the experiments at lower pressures reaches only the most calcic end of this range at the lowest temperatures explored.) In addition, the plagioclase in the anorthosites has similar Or content to our 9·3 kbar plagioclase. Thus, these experiments also support the formation of the plagioclase of the anorthosite bodies of the LAC at elevated pressure during crystallization of a tholeiitic or HAG-like parental liquid.

Implications for the ocean island tholeiitic series

The experiments carried out on I260 at '0 kbar' produced liquids that are markedly similar in bulk composition to basaltic rocks found in the ocean island tholeiitic series, characterized by a silica-enrichment trend in the residual liquids. There are, however, some deviations in the experimental liquid compositions at '0 kbar' from the natural ocean island tholeiitic series shown. Potassium deviates fairly significantly from the natural trend during crystallization, owing to the relatively high starting K_2O content of I260 compared with that of the least-evolved rocks of the ocean island tholeiitic series. TiO_2 contents of low-temperature residual liquids lie slightly above the trend, and FeO_T plots just barely below the ocean island tholeiitic trend. The deviations in TiO_2 and FeO_T may result from the relatively high fO_2 of the '0 kbar' experiments.

How much of this silica-enrichment trend, however, is an effect of pressure rather than an effect of fO_2? Because the experiments conducted at '0 kbar' were conducted at a higher fO_2 than those at higher pressures, fO_2 represents a variable in addition to pressure that must be considered. Higher fO_2 would lead to increased magnetite component in the spinel, which would lead to a decrease in the amount of olivine and pyroxene that can form, resulting in a greater amount of silica enrichment. However, the amount of spinel crystallizing in these experiments is very low. Calculations in which all of the Fe in the spinel is removed to make more olivine still indicated significant silica enrichment of the residual liquid. Therefore, we believe it is primarily a pressure effect that produces the compositional differences between the two trends.

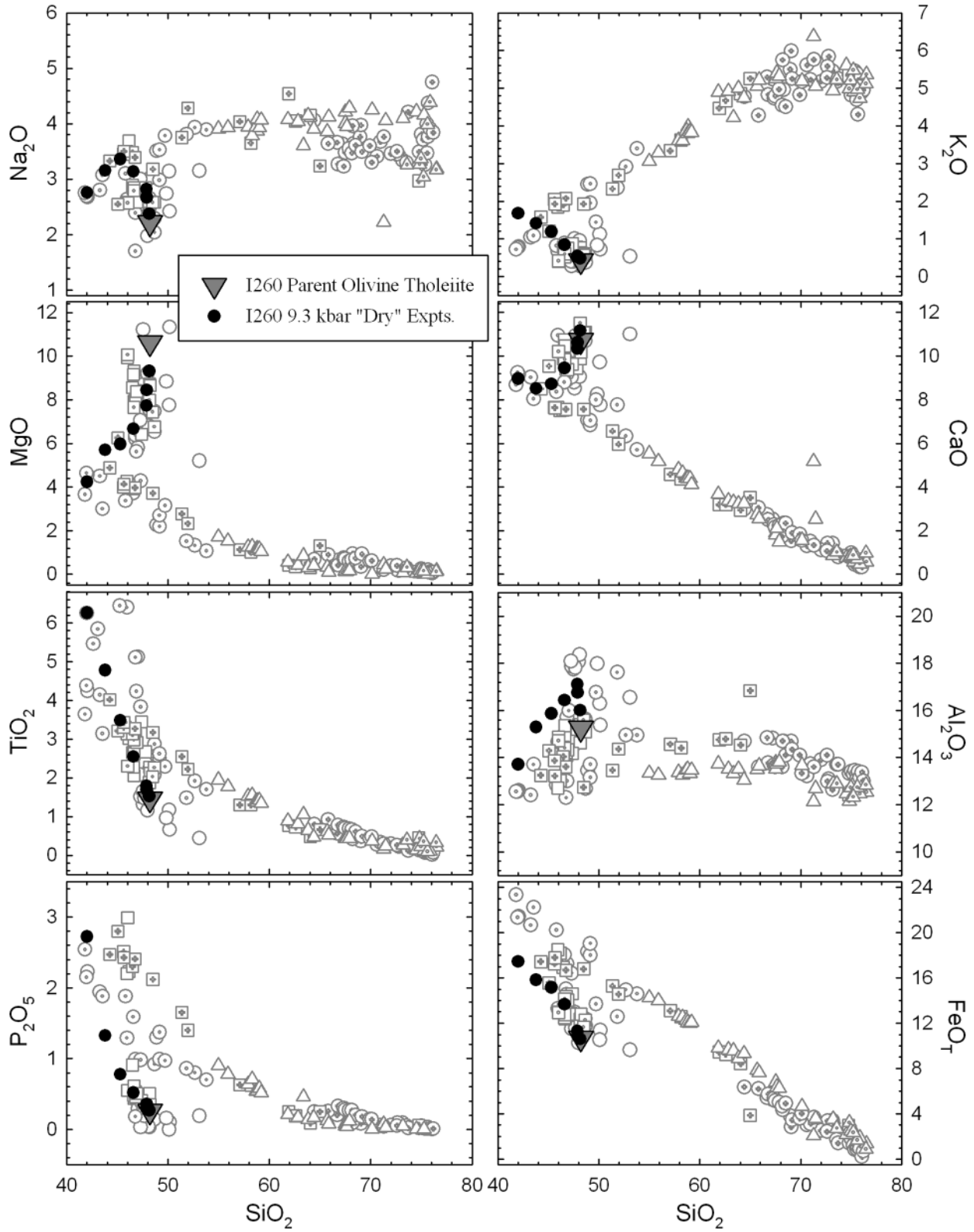

Fig. 7. Major element Harker variation diagrams of residual liquid compositions of experiments on 'dry' I260 (gray triangle) at 9·3 kbar (black circles). Other symbols are as in Fig. 1.

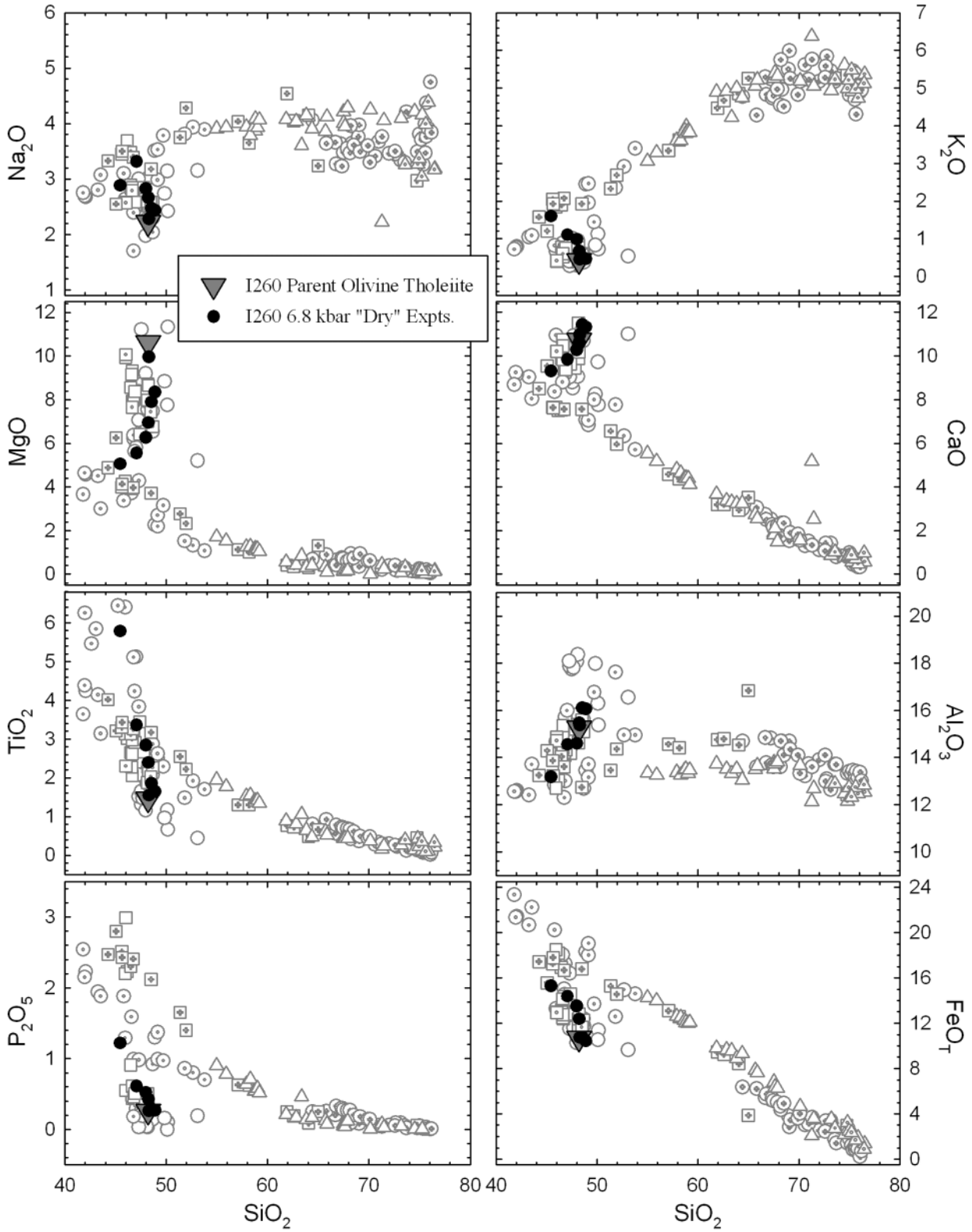

Fig. 8. Major element Harker variation diagrams of residual liquid compositions of experiments on 'dry' I260 (gray triangle) at 6·8 kbar (black circles). Other symbols are as in Fig. 1.

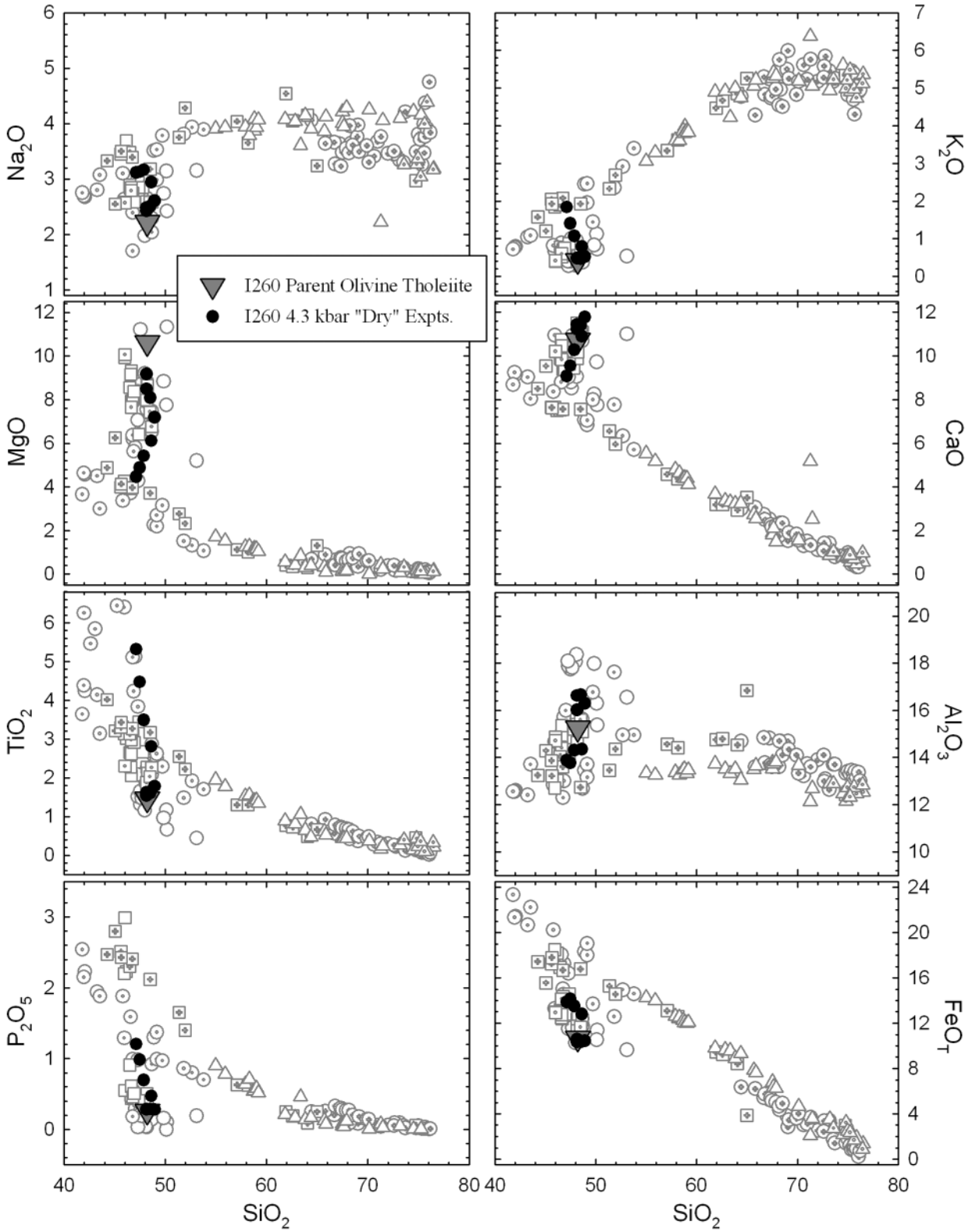

Fig. 9. Major element Harker variation diagrams of residual liquid compositions of experiments on 'dry' I260 (gray triangle) at 4·3 kbar (black circles). Other symbols are as in Fig. 1.

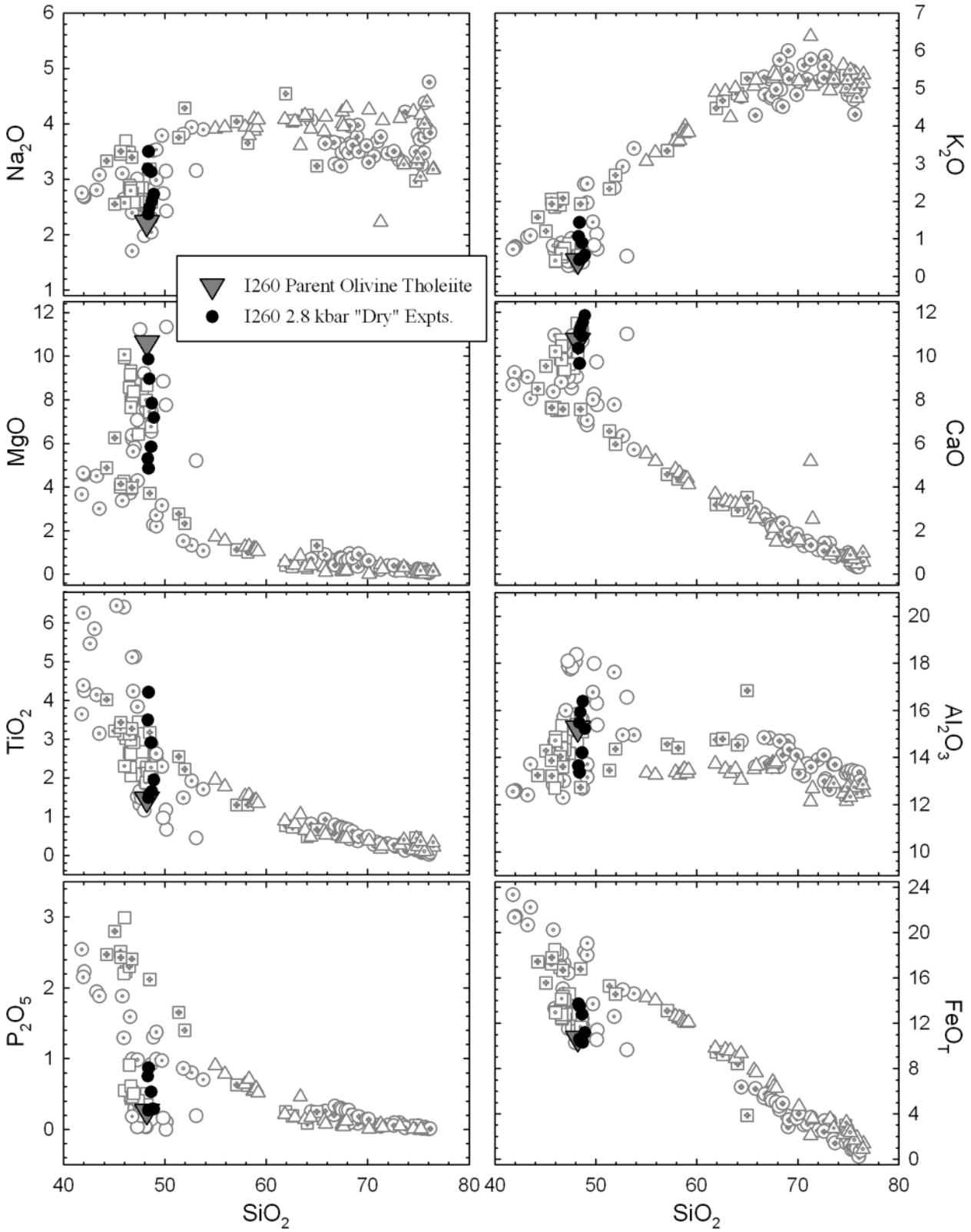

Fig. 10. Major element Harker variation diagrams of residual liquid compositions of experiments on 'dry' I260 (gray triangle) at 2·8 kbar (black circles). Other symbols are as in Fig. 1.

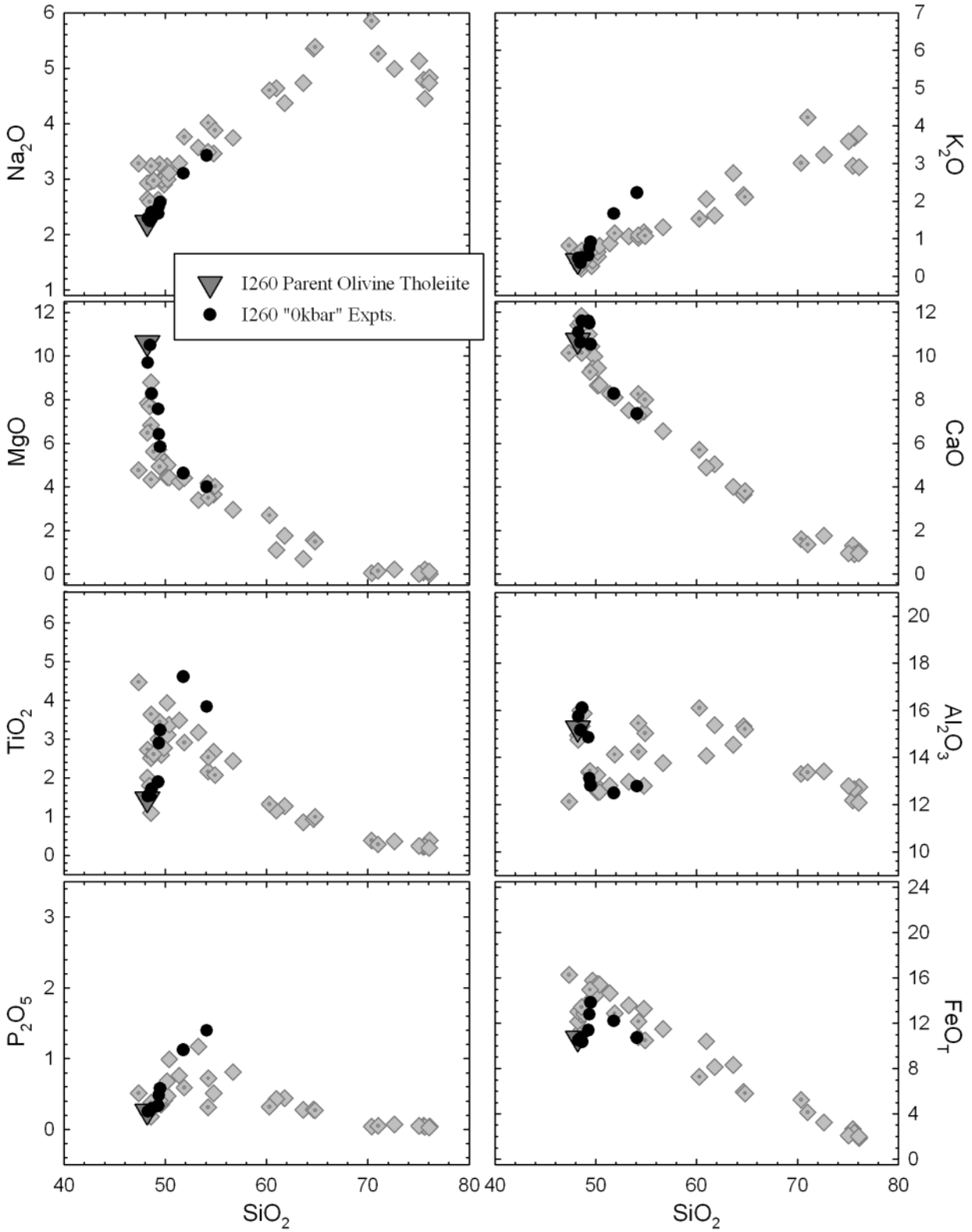

Fig. 11. Major element Harker variation diagrams of residual liquid compositions of experiments on 'dry' I260 (gray triangle) at '0 kbar' (black circles). Other symbols are as in Fig. 1.

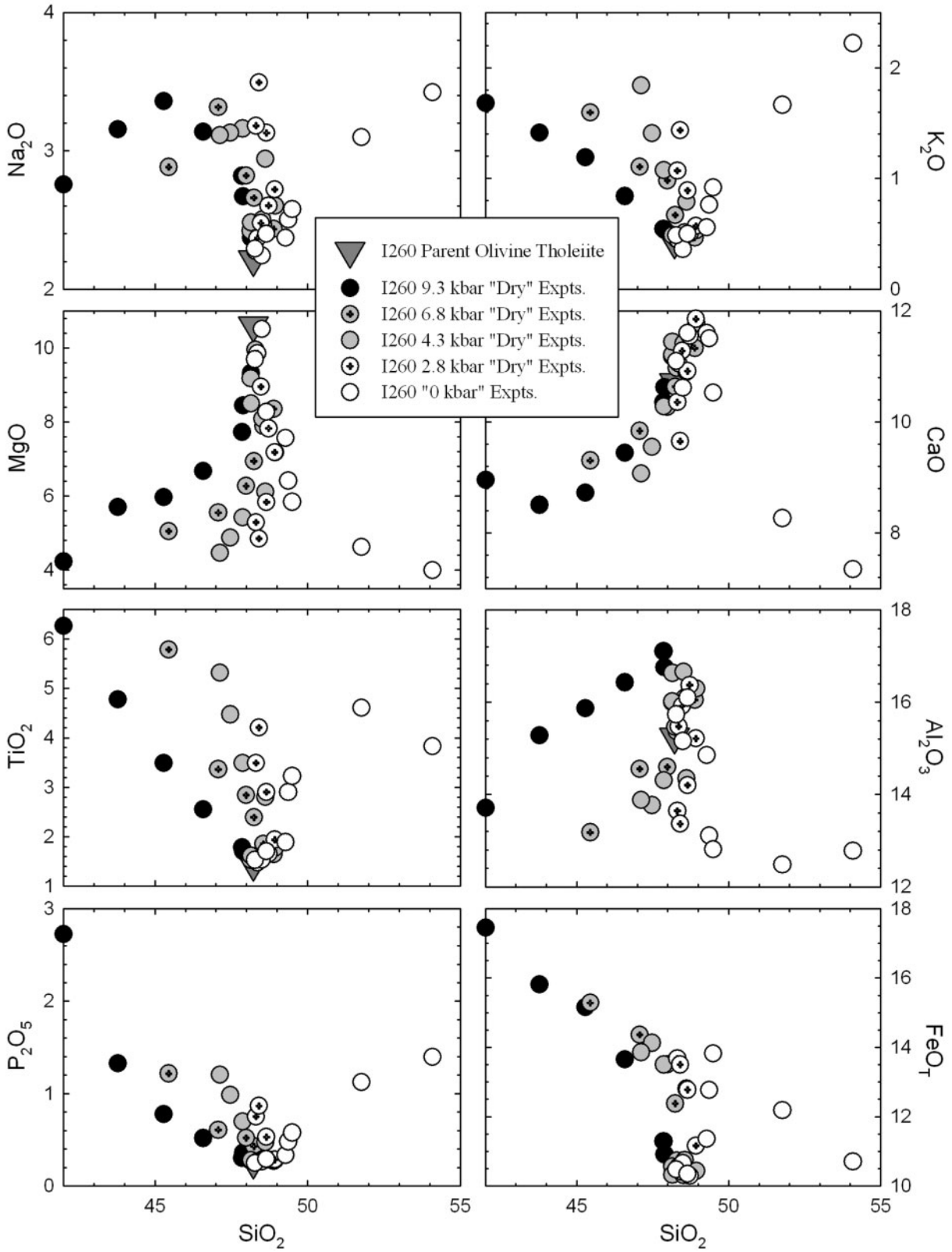

Fig. 12. Major element Harker variation diagrams of residual liquid compositions of experiments on 'dry' I260 (gray triangle) at 9·3 kbar (black circles), 6·8 kbar (gray circles with crosshairs), 4·3 kbar (gray circles), 2·8 kbar (open circles with crosshairs), and '0 kbar' (open circles).

The mineral assemblages produced experimentally at '0 kbar' agree well with the observed phenocryst phases from the natural rocks. Olivine tholeiite, tholeiite and basaltic andesite from Thingmuli (Iceland) contain phenocrysts of plagioclase ranging in composition from bytownite to labradorite, in addition to rare olivine ($\sim Fo_{75}$) and augite ($\sim Wo_{40}En_{45}$) phenocrysts (Carmichael, 1964). Pinzon (Galapagos) basaltic rocks contain plagioclase phenocrysts ranging in composition from An_{76} to An_{63}, olivine phenocrysts ranging from Fo_{85} to Fo_{57}, phenocrystic augite ranging from $Wo_{43}En_{47}$ to $Wo_{38}En_{42}$, and occasional phenocrysts of Fe–Ti oxides (Baitis & Lindstrom, 1980). Phenocryst assemblages in basaltic rocks from Volcan Alcedo (Galapagos) include plagioclase ($An_{84–61}$), augite ($Wo_{45–41}En_{46–45}$), olivine ($Fo_{85–63}$), and small amounts of Ti-magnetite (Geist *et al.*, 1995). The experimental plagioclase in these experiments ranges in composition from An_{78} to An_{67}, olivines range from Fo_{87} to Fo_{71}, and augites range from $Wo_{40}En_{49}$ to $Wo_{38}En_{44}$. An Fe–Ti oxide phase was also crystallized experimentally.

The similarities between natural bulk lava compositions and experimental residual liquids as well as between experimental and natural phenocryst assemblages support the results of Spulber & Rutherford (1983) suggesting that these rocks form by shallow crystallization of a tholeiitic parental magma.

CONCLUSIONS

Crystallization of a 'dry' olivine tholeiite parental non-primitive melt at various levels within the crust produces markedly different mineral assemblages and residual liquids. Olivine tholeiite of the type found in the Snake River Plain can produce liquid compositions similar to bulk-rock compositions found in both the potassic silica-saturated alkalic series, such as those from the Snake River Plain–Craters of the Moon and Laramie Anorthosite Complex by crystallization at elevated pressures. It can also produce the ocean island tholeiitic series, exemplified by rocks from Iceland and the Galapagos, via crystallization at low pressure.

We suggest here that pressure-induced changes in phase relations—such as early stability of intermediate plagioclase and clinopyroxene at elevated pressure, and early stability of more anorthitic plagioclase at lower pressure as well as late crystallization of pyroxene—are the primary factors that give rise to the compositional diversity in residual liquids of these two suite types. The differences in oxygen fugacity simply cannot account for the differences in liquid evolution observed.

Some variations in the olivine tholeiite compositions that give rise to these two suite types do appear to exist, however. These can be seen by the emanation of the ocean island tholeiitic series from a more sodic tholeiite and the silica-saturated potassic series from a slightly more potassic tholeiite. These differences in olivine tholeiite may arise secondarily, such as through crustal contamination, and may not be the result of differences in source compositions. The primary pressure-dependent liquid evolutionary trends appear robust through this variation.

In addition to the slight compositional variations in the olivine tholeiite of the two suite types, there are differences in oxygen fugacity. However, these differences may also reflect secondary processes, and need not imply different source characteristics. The redox state of ascending magma may change depending upon the nature of the buffering assemblages in the hosting rocks. If ferrous–ferric equilibria dictate the fO_2 of the upper mantle and crust (Ballhaus & Frost, 1994), and the melts ascend slowly enough to maintain equilibrium with the hosting rocks, the melts will become more oxidized at shallower levels. Thus, the same parental tholeiite may be more oxidized at shallower depths than at high pressure, and this change in fO_2 is brought about not by differences in source region chemistry, but rather by differences in environment.

The results of this study indicate that the broad compositional diversity of dry intraplate basaltic magmas may arise from a single parental magma composition as a result of crystal–liquid differentiation processes at different pressures and does not necessitate source region heterogeneity.

ACKNOWLEDGEMENTS

The authors would like to gratefully acknowledge the helpful and constructive reviews by Dave Walker, Tony Morse, and Eric Christiansen. Their comments, along with those of editor Ron Frost, helped to greatly improve the quality of this manuscript. The authors acknowledge the financial support of NSF grant EAR 0003443 to D.H.L. and H.N.

REFERENCES

Abbott, M. J. (1969). Petrology of the Nandewar Volcano, N.S.W., Australia. *Contributions to Mineralogy and Petrology* **20**, 115–134.

Andersen, D. J., Lindsley, D. H. & Davidson, P. M. (1993). QUILF—a Pascal program to assess equilibria among Fe–Mg–Mn–Ti oxides, pyroxenes, olivine, and quartz. *Computers and Geosciences* **19**, 1333–1350.

Baitis, H. W. & Lindstrom, M. M. (1980). Geology, petrography, and petrology of Pinzon Island, Galapagos archipelago. *Contributions to Mineralogy and Petrology* **72**, 367–386.

Baker, P. E., Buckley, F. & Holland, J. G. (1974). Petrology and geochemistry of Easter Island. *Contributions to Mineralogy and Petrology* **44**, 85–100.

Ballhaus, C. & Frost, B. R. (1994). The generation of oxidized CO_2-bearing basaltic melts from reduced CH_4-bearing upper-mantle sources. *Geochimica et Cosmochimica Acta* **58**, 4931–4940.

Carmichael, I. S. E. (1964). The petrology of Thingmuli, a Tertiary volcano in Eastern Iceland. *Journal of Petrology* **5**, 435–460.

Carr, M. J. (2002). *IgPet for Windows*. Somerset, NJ: Terra Softa Inc.

Christiansen, E. H. & McCurry, M. (2006). Contrasting origins of Cenozoic silicic volcanic rocks from the Western Cordillera of the United States. *Bulletin of Volcanology* (in press).

Dixon, J. E., Stolper, E. M. & Holloway, J. R. (1995). An experimental study of water and carbon dioxide solubilities in mid-ocean ridge basaltic liquids. Part 1: Calibration and solubility models. *Journal of Petrology* **36**, 1607–1631.

Duke, J. M. (1976). Distribution of the period four transition elements among olivine, calcic clinopyroxene and mafic silicate liquid; experimental results. *Journal of Petrology* **17**, 499–521.

Eugster, H. P. & Skippen, G. B. (1967). Igneous and metamorphic reactions involving gas equilibria. In: Abelson, P. H. (ed.) *Researches in Geochemistry*. New York: John Wiley, pp. 492–520.

Filiberto, J. & Nekvasil, H. (2003). Linking tholeiites and silica-undersaturated alkalic rocks: an experimental study. *Geological Society of America, Abstracts with Programs* **35**, 632.

Fram, M. S. & Longhi, J. (1992). Phase equilibria of dikes associated with Proterozoic anorthosite complexes. *American Mineralogist* **77**, 605–616.

Frey, F. A., Garcia, M. O., Wise, W. S., Kennedy, A., Gurriet, P. & Albarede, F. (1991). The evolution of Mauna-Kea Volcano, Hawaii—petrogenesis of tholeiitic and alkalic basalts. *Journal of Geophysical Research—Solid Earth and Planets* **96**, 14347–14375.

Frost, C. D. & Frost, B. R. (1997). Reduced rapakivi-type granites: the tholeiite connection. *Geology* **25**, 647–650.

Frost, B. R. & Lindsley, D. H. (1992). Equilibria among Fe–Ti oxides, pyroxenes, olivine, and quartz: Part II. Application. *American Mineralogist* **77**, 1004–1020.

Frost, B. R., Frost, C. D., Lindsley, D. H., Scoates, J. S. & Mitchell, J. N. (1993). The Laramie Anorthosite Complex and Sherman Batholith: geology, evolution, and theories of origin. In: Snoke, A. W., Steidtmann, J. R. & Roberts, S. (eds) *Geology of Wyoming. Geological Survey of Wyoming Memoir* **5**, 118–161.

Frost, C. D., Frost, B. R., Chamberlain, K. R. & Edwards, B. R. (1999). Petrogenesis of the 1·43 Ga Sherman batholith, SE Wyoming, USA: a reduced, rapakivi-type anorogenic granite. *Journal of Petrology* **40**, 1771–1802.

Geist, D., Howard, K. A. & Larson, P. (1995). The generation of oceanic rhyolites by crystal fractionation—the basalt–rhyolite association at Volcan Alcedo, Galapagos archipelago. *Journal of Petrology* **36**, 965–982.

Ghiorso, M. S. & Sack, R. O. (1995). Chemical mass-transfer in magmatic processes IV. A revised and internally consistent thermodynamic model for the interpolation and extrapolation of liquid–solid equilibria in magmatic systems at elevated temperatures and pressures. *Contributions to Mineralogy and Petrology* **119**, 197–212.

Ghiorso, M. S., Hirschmann, M. M., Reiners, P. W. & Kress, V. C. (2002). The pMELTS: a revision of MELTS for improved calculation of phase relations and major element partitioning related to partial melting of the mantle to 3 GPa. *Geochemistry, Geophysics, Geosystems* **3**, doi: 10.1029/2001GC000217, 36 pp.

Haase, K. M., Stoffers, P. & Garbe-Schönberg, C. D. (1997). The petrogenetic evolution of lavas from Easter Island and neighbouring seamounts, near-ridge hotspot volcanoes in the SE Pacific. *Journal of Petrology* **38**, 785–813.

Harris, C. (1983). The petrology of lavas and associated plutonic inclusions of Ascension Island. *Journal of Petrology* **24**, 424–470.

Irvine, T. N. & Baragar, W. R. A. (1971). Guide to chemical classification of common volcanic rocks. *Canadian Journal of Earth Sciences* **8**, 523–548.

Kuntz, M. A., Covington, H. R. & Schorr, L. J. (1992). An overview of basaltic volcanism of the eastern Snake River plain, Idaho. In: Link, P. K., Kuntz, M. A. & Platt, L. B. (eds) *Regional Geology of Eastern Idaho and Western Wyoming, Geological Society of America, Memoir* **179**, 227–267 .

Leeman, W. P. (1982*a*). Rhyolites of the Snake River Plain—Yellowstone Plateau province, Idaho and Wyoming; a summary of petrogenetic models. In: Bonnichsen, B. & Breckenridge, R. M. (eds). *Cenozoic Geology of Idaho. Bulletin—Idaho Bureau of Mines and Geology* **26**, 203–212.

Leeman, W. P. (1982b). Olivine tholeiitic basalts of the Snake River Plain, Idaho. In: Bonnichsen, B. & Breckenridge, R. M. (eds). *Cenozoic Geology of Idaho. Bulletin—Idaho Bureau of Mines and Geology* **26**, 181–191.

Leeman, W. P. & Vitaliano, C. J. (1976). Petrology of McKinney Basalt, Snake River Plain, Idaho. *Geological Society of America Bulletin* **87**, 1777–1792.

Leeman, W. P., Vitaliano, C. J. & Prinz, M. (1976). Evolved lavas from the Snake River Plain—Craters of the Moon National Monument, Idaho. *Contributions to Mineralogy and Petrology* **56**, 35–60.

Leroex, A. P. (1985). Geochemistry, mineralogy and magmatic evolution of the basaltic and trachytic lavas from Gough Island, South Atlantic. *Journal of Petrology* **26**, 149–186.

Lindsley, D. H. (1983). Pyroxene thermometry. *American Mineralogist* **68**, 477–493.

Lindsley, D. H. & Andersen, D. J. (1983). A two-pyroxene thermometer. In: Boynton, W. V. & Ahrens, T. J. (eds) *Proceedings of the 13th Lunar and Planetary Science Conference*. Houston, TX: Lunar and Planetary Institute, pp. A887–A906.

Litvin, V. Y. (2002). *Application of fractional crystallization to the origin of continental tholeiitic suites*. Stony Brook, NY: State University of New York at Stony Brook, Department of Geosciences, 138 pp.

Macdonald, R., Sparks, R. S. J., Sigurdsson, H., Mattey, D. P., McGarvie, D. W. & Smith, R. L. (1987). The 1875 eruption of Askja Volcano, Iceland—combined fractional crystallization and selective contamination in the generation of rhyolitic magma. *Mineralogical Magazine* **51**, 183–202.

Mandeville, C. W., Webster, J. D., Rutherford, M. J., Taylor, B. E., Timbal, A. & Faure, K. (2002). Determination of molar absorptivities for infrared absorption bands of H_2O in andesitic glasses. *American Mineralogist* **87**, 813–821.

McCurry, M., Hackett, W. R. & Hayden, K. (1999). Cedar Butte and cogenetic Quaternary rhyolite domes of the Eastern Snake River Plain. In: Hughes, S. S. & Thackray, G. D. (eds) *Guidebook to the Geology of Eastern Idaho*. Idaho Museum of Natural History. Idaho: Pocatello, pp. 169–179.

McCurry, M., Hayden, K. P., Morse, L. H. & Mertzman, S. (2006). Genesis of post-hotspot A-type rhyolite of the Eastern Snake River Plain volcanic field by extreme fractional crystallization of olivine tholeiite basalt. *Bulletin of Volcanology* (in press).

Mitchell, J. N., Scoates, J. S. & Frost, C. D. (1995). High-Al gabbros in the Laramie Anorthosite Complex, Wyoming—implications for the composition of melts parental to Proterozoic anorthosite. *Contributions to Mineralogy and Petrology* **119**, 166–180.

Mitchell, J. N., Scoates, J. S., Frost, C. D. & Kolker, A. (1996). The geochemical evolution of anorthosite residual magmas in the Laramie Anorthosite Complex, Wyoming. *Journal of Petrology* **37**, 637–660.

Nekvasil, H., Simon, A. & Lindsley, D. H. (2000). Crystal fractionation and the evolution of intra-plate hy-normative igneous suites: insights from their feldspars. *Journal of Petrology* **41**, 1743–1757.

Nekvasil, H., Lindsley, D. H., Whitaker, M. L., Filiberto, J., DiFrancesco, N. J., Rossier, L. & Horn, J. (2003). Tholeiites, anorthosites, potassic granites, sodic trachytes, and tephriphonolites: is there a link? *Geological Society of America, Abstracts with Programs* **35**, 395.

Nekvasil, H., Dondolini, A., Horn, J., Filiberto, J., Long, H. & Lindsley, D. H. (2004). The origin and evolution of silica-saturated alkalic suites: an experimental study. *Journal of Petrology* **45**, 693–721.

Newton, R. C., Charlu, T. V. & Kleppa, O. J. (1974). Calorimetric investigation of stability of anhydrous magnesium cordierite with application to granulite facies metamorphism. *Contributions to Mineralogy and Petrology* **44**, 295–311.

Peng, X. H. & Humphreys, E. D. (1998). Crustal velocity structure across the eastern Snake River Plain and the Yellowstone swell. *Journal of Geophysical Research—Solid Earth* **103**, 7171–7186.

Reed, M. F., Bartholomay, R. C. & Hughes, S. S. (1997). Geochemistry and stratigraphic correlation of basalt lavas beneath the Idaho Chemical Processing Plant, Idaho National Engineering Laboratory. *Environmental Geology* **30**, 108–118.

Scoates, J. S., Frost, C. D., Mitchell, J. N., Lindsley, D. H. & Frost, B. R. (1996). Residual-liquid origin for a monzonitic intrusion in a mid-Proterozoic anorthosite complex: the Sybille intrusion, Laramie Anorthosite Complex, Wyoming. *Geological Society of America Bulletin* **108**, 1357–1371.

Scoates, J. S., Lindsley, D. H., van der Kolk, D. & Anderson, K. (1999). Fractional crystallization experiments on a candidate parental magma to anorthosite. *EOS Transactions, American Geophysical Union* **80**, F1096.

Sparlin, M. A., Braile, L. W. & Smith, R. B. (1982). Crustal structure of the Eastern Snake River Plain determined from ray trace modeling of seismic refraction data. *Journal of Geophysical Research* **87**, 2619–2633.

Spulber, S. D. & Rutherford, M. J. (1983). The origin of rhyolite and plagiogranite in oceanic crust—an experimental study. *Journal of Petrology* **24**, 1–25.

Stolz, A. J. (1985). The role of fractional crystallization in the evolution of the Nandewar Volcano, northeastern New South Wales, Australia. *Journal of Petrology* **26**, 1002–1026.

Stout, M. Z. & Nicholls, J. (1977). Mineralogy and petrology of Quaternary lavas from the Snake River Plain, Idaho. *Canadian Journal of Earth Sciences* **14**, 2140–2156.

Stout, M. Z., Nicholls, J. & Kuntz, M. A. (1994). Petrological and mineralogical variations in 2500–2000 yr B.P. lava flows, Craters of the Moon lava field, Idaho. *Journal of Petrology* **35**, 1681–1715.

Takahashi, E. (1978). Partitioning of Ni^{2+}, Co^{2+}, Fe^{2+}, Mn^{2+} and Mg^{2+} between olivine and silicate melts—compositional dependence of partition coefficient. *Geochimica et Cosmochimica Acta* **42**, 1829–1844.

Thompson, R. N. (1975). Primary basalts and magma genesis II. Snake River Plain, Idaho, USA. *Contributions to Mineralogy and Petrology* **52**, 213–232.

Villiger, S., Ulmer, P., Muntener, O. & Thompson, A. B. (2004). The liquid line of descent of anhydrous, mantle-derived, tholeiitic liquids by fractional and equilibrium crystallization—an experimental study at 1·0 GPa. *Journal of Petrology* **45**, 2369–2388.

Whitaker, M. L., Nekvasil, H. & Lindsley, D. H. (2004). Can fractionation of an olivine tholeiite give rise to potassic rhyolites? *Geological Society of America, Abstracts with Programs* **36**, 25.

Whitaker, M. L., Nekvasil, H., Lindsley, D. H. & McCurry, M. (2006). Can crystallization of olivine tholeiite give rise to potassic rhyolites? An experimental investigation. *Bulletin of Volcanology* (in press).

Yoder, H. S. & Tilley, C. E. (1962). Origin of basalt magmas: an experimental study of natural and synthetic rock systems. *Journal of Petrology* **3**, 342–532.